Decremental Response to High-Frequency Trains of Acetylcholine Pulses but Unaltered Fractional Ca^{2+} Currents in a Panel of "Slow-Channel Syndrome" Nicotinic Receptor Mutants

Sergio Elenes, Michael Decker, Gisela D. Cymes, and Claudio Grosman

Department of Molecular and Integrative Physiology, Center for Biophysics and Computational Biology, and Neuroscience Program, University of Illinois at Urbana-Champaign, Urbana, IL 61801

The slow-channel congenital myasthenic syndrome (SCCMS) is a disorder of the neuromuscular junction caused by gain-of-function mutations to the muscle nicotinic acetylcholine (ACh) receptor (AChR). Although it is clear that the slower deactivation time course of the ACh-elicited currents plays a central role in the etiology of this disease, it has been suggested that other abnormal properties of these mutant receptors may also be critical in this respect. We characterized the kinetics of a panel of five SCCMS AChRs (αS269I, βV266M, εL221F, εT264P, and εL269F) at the ensemble level in rapidly perfused outside-out patches. We found that, for all of these mutants, the peak-current amplitude decreases along trains of nearly saturating ACh pulses delivered at physiologically relevant frequencies in a manner that is consistent with enhanced entry into desensitization during the prolonged deactivation phase. This suggests that the increasingly reduced availability of activatable AChRs upon repetitive stimulation may well contribute to the fatigability and weakness of skeletal muscle that characterize this disease. Also, these results emphasize the importance of explicitly accounting for entry into desensitization as one of the pathways for burst termination, if meaningful mechanistic insight is to be inferred from the study of the effect of these naturally occurring mutations on channel function. Applying a novel single-channel–based approach to estimate the contribution of Ca^{2+} to the total cation currents, we also found that none of these mutants affects the Ca^{2+}-conduction properties of the AChR to an extent that seems to be of physiological importance. Our estimate of the Ca^{2+}-carried component of the total (inward) conductance of wild-type and SCCMS AChRs in the presence of 150 mM Na^{+}, 1.8 mM Ca^{2+}, and 1.7 mM Mg^{2+} on the extracellular side of cell-attached patches turned out be in the 5.0–9.4 pS range, representing a fractional Ca^{2+} current of ∼14%, on average. Remarkably, these values are nearly identical to those we estimated for the NR1-NR2A *N*-methyl-D-aspartate receptor (NMDAR), which has generally been considered to be the main neurotransmitter-gated pathway of Ca^{2+} entry into the cell. Our estimate of the rat NMDAR Ca^{2+} conductance (using the same single-channel approach as for the AChR but in the nominal absence of extracellular Mg^{2+}) was 7.9 pS, corresponding to a fractional Ca^{2+} current of 13%.

The Journal of General Physiology

INTRODUCTION

Naturally occurring mutations to the muscle nicotinic acetylcholine (ACh) receptor (AChR) are one of the multiple possible causes of congenital myasthenic syndrome, a genetically and phenotypically heterogeneous disease of the neuromuscular junction that is typically manifest as increased fatigability and weakness of skeletal muscle with a distinctive electromyographic pattern (Engel et al., 2003; Hantai et al., 2004). Specifically, AChR mutations that prolong the mean duration of individual channel activations (that is, the duration of a "burst of single-channel openings"; Colquhoun and Sakmann, 1985) cause a particular type of congenital myasthenic syndrome known as "slow-channel syndrome," in which the time course of the endplate-current decay is abnormally slow. Unsurprisingly, the study of the functional impact of these gain-of-function mutations has elicited considerable interest both as a step toward an understanding of the molecular basis of this type of neuromuscular disorder and as an opportunity to reveal novel properties of the AChR that may be unlikely to be stumbled upon as a result of unguided mutagenesis approaches.

Although our knowledge of the link between the observed quantitative changes in AChR function and the different clinical and histological manifestations of this pathology remains incomplete, it is clear that the slower deactivation time constant of the mutated AChRs is key. On the one hand, the prolonged time constant of the synaptic-current decay may lead to the summation of inward currents upon repetitive motor-neuron firing, resulting in sustained endplate depolarization, inactivation

Correspondence to Claudio Grosman: grosman@life.uiuc.edu

S. Elenes's present address is University Center for Biomedical Research, University of Colima, Colima, 28045, Mexico.

Abbreviations used in this paper: ACh, acetylcholine; AChR, ACh receptor; cDNA, complementary DNA; NMDAR, *N*-methyl-D-aspartate receptor.

The Rockefeller University Press $30.00
J. Gen. Physiol. Vol. 133 No. 2 151–169
www.jgp.org/cgi/doi/10.1085/jgp.200810089

of muscle voltage-dependent Na^+ channels, and, ultimately, neuromuscular blockade. On the other hand, the prolonged currents could result in an excessive Ca^{2+} load with potentially cytotoxic effects (Leonard and Salpeter, 1979), a phenomenon that may well underlie the degeneration of junctional folds typically observed in skeletal muscle biopsies from affected individuals (Gomez et al., 1997; Groshong et al., 2007).

Another aspect of AChR function that is severely compromised upon gain-of-function mutations (that is, mutations that slow down channel closing, speed up channel opening, and/or slow down ACh dissociation from the transmitter-binding sites in the closed state) is the ability to respond reliably to trains of high-frequency stimulation. Using outside-out patch clamp recordings from heterologously expressed receptors (harboring mutations that increase the diliganded-gating equilibrium constant but leave the kinetics of agonist-dissociation essentially unaffected; Grosman and Auerbach, 2000, 2001) and a piezo-electrically driven, fast perfusion system, we found that the response to repetitive, brief (<1-ms) applications of ACh decreases gradually along the train, with the extent of this "depression" increasing as the frequency of the train does (Elenes et al., 2006). Furthermore, we found that (for the different constructs and at a given stimulation frequency) the slower the deactivation time course, the deeper the extent of this depression. In mechanistic terms, these observations indicate that: (a) bursts of diliganded openings can terminate not only through ligand dissociation, but also through entry into desensitization; (b) the kinetics of recovery from desensitization are such that its extent is sensitive to the duration of the applied interpulse intervals (tens to hundreds of milliseconds); and (c) desensitization can proceed from the open-diliganded conformation in such a way that mutations that slow down deactivation by increasing the $CA_2 \rightleftharpoons OA_2$ gating equilibrium constant can increase the contribution of entry into desensitization to the termination of a burst of diliganded openings (Fig. 1).

A slower deactivation (or, its single-channel counterpart, a prolonged mean burst duration; Colquhoun et al., 1997; Wyllie et al., 1998) alone, however, need not be accompanied by a decremental response to high-frequency trains of agonist pulses because mutations may also affect the kinetics of desensitization. Certainly, a slower rate of entry into desensitization and/or a faster rate of recovery from it can compensate for the effect of a slower deactivation time constant, and thus, may result in a rather uniform response to repetitive agonist applications. One of the questions we address here is, precisely, whether the slow deactivation of naturally occurring, slow-channel syndrome AChR mutants leads to a progressive reduction of peak currents upon repetitive exposure to ACh. The importance of a positive result would be twofold. First, such depression could compromise the safety margin of the motor endplate, and thus, could contribute to the deranged neuromuscular transmission and ensuing clinical symptoms. Second, such depression would indicate that a sensible study of the impact of these mutations on the AChR's function could not be done unless the desensitization phenomenon is explicitly accounted for in the reaction schemes used to interpret the observations. Needless to say, kinetic models that do not include desensitized states predict a uniform response to trains of ACh pulses regardless of the value of the mean burst duration, as if the only pathway out of a burst of activity were agonist dissociation.

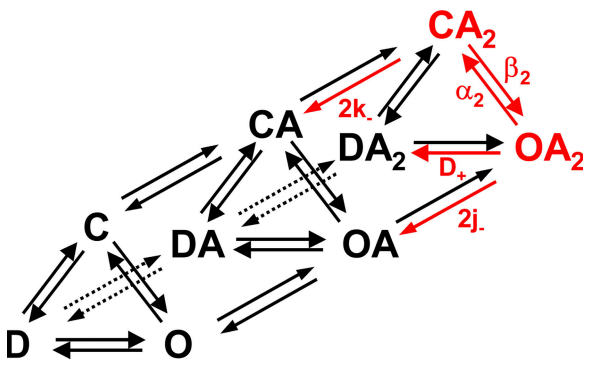

Figure 1. A reaction mechanism for the muscle AChR. C, O, and D denote the closed, open, and desensitized conformations of the channel, respectively, whereas A denotes a molecule of ACh. The red arrows identify the subset of rate constants that, according to Eq. 1, determine the kinetics of the macroscopic current decay through the muscle AChR during channel deactivation (or, equivalently, the mean duration of a burst of single-channel diliganded openings). The states indicated in red (CA_2 and OA_2) are those that would interconvert during a burst of diliganded openings.

The other question we address here is whether the contribution of Ca^{2+} to the total cation influx through the muscle AChR (that is, the "fractional Ca^{2+} current") is altered in "slow-channel" mutants. By combining whole cell patch clamp and Ca^{2+}-indicator fluorescence recordings (Thayer et al., 1988; Neher and Augustine, 1992; Zhou and Neher, 1993; Vernino et al., 1994; Schneggenburger, 1996), it has been recently reported that the fractional Ca^{2+} currents through some of these disease-causing AChRs are twice as high as those through the wild-type channel (Di Castro et al., 2007), a notion that would have strong implications not only for the delineation of the molecular basis of the disease, but also for our understanding of the molecular determinants of Ca^{2+} conduction through this channel. However, these measurements are inherently complex and require that a large number of variables be strictly controlled. The method, thus, becomes prone to large errors (Zhou and Neher, 1993) as, perhaps, reflected in the disparate values reported by different studies on the same types of ion channel (for example, Schneggenburger et al., 1993; Schneggenburger, 1996). Here, we present a simple alternative to tackle this problem. Our

approach relies solely on single-channel current measurements and avoids altogether the calculation of permeability ratios from reversal potentials estimated under nonphysiological ion conditions.

MATERIALS AND METHODS

Complementary DNA (cDNA) Clones, Mutagenesis, and Heterologous Expression

cDNAs encoding for the α1, β1, δ, γ, and ε subunits of the mouse muscle AChR were provided by S.M. Sine (Mayo Clinic College of Medicine, Rochester, MN), whereas those encoding for the α1, β1, δ, and ε subunits of the human muscle counterpart were provided by L.G. Sivilotti (University College London, London, England, UK). cDNAs encoding for the NR1 (splice variant NR1-1a; Hollmann et al., 1993) and NR2A subunits of the rat *N*-methyl-D-aspartate receptor (NMDAR) were provided by J. Woodward (Medical University of South Carolina, Charleston, SC). HEK-293 cells were transiently transfected using a calcium-phosphate precipitation method (Purohit and Grosman, 2006). In the case of the cells expressing the NMDAR, the antagonist DL-2-amino-5-phosphonovaleric acid (final concentration, 200 μM) was added to the fresh culture medium used to replace the calcium-phosphate–DNA mixture after the overnight incubation. All the mutations to the muscle AChR were engineered on the mouse clones with the QuikChange site-directed mutagenesis kit (Agilent Technologies) and were confirmed by dideoxy sequencing. The naturally occurring "gain-of-function" mutations were αS269I, βV266M, εL221F, εT264P, and εL269F. The naturally occurring "loss-of-function" mutations were δD59K and εP121L. Unless otherwise stated, the adult muscle type of AChR was studied (that is, receptors containing α1, β1, δ, and ε subunits).

Electrophysiological Recordings

Step changes in the concentration of ACh applied to outside-out patches were achieved by the rapid switching of two solutions flowing from either barrel of a piece of "theta-type" capillary glass tubing (Hilgenberg), essentially as described by Jonas (1995). The theta tube was mounted on a piezo-electric device (Burleigh-LSS-3100; Exfo), the movement of which was controlled by a computer using a Digidata 1322A interface (MDS Analytical Technologies) and pClamp 9.0 software (MDS Analytical Technologies). To minimize distortions in the time course of the solution exchange, the computer-generated rectangular waveforms (brief pulses, long pulses, and trains of brief pulses) were low-pass filtered (f_c = 150–180 Hz) before being applied to the piezo-electric device. The recording chamber (designed in-house) contained two compartments that could be isolated from one another by reducing the total volume of solution in the chamber. One compartment was used for placing the poly-L-lysine–coated coverslip with cells, whereas the other one (the "recording compartment") was used for placing the theta tube and the patch pipette during recordings. The latter compartment was continuously perfused using a gravity-fed system, whereas the solutions flowing through the theta tube were pressure driven (ALA BPS-8; ALA Scientific Instruments). To estimate the time course of the solution exchange, the change in liquid-junction potential was measured with an open-tip patch pipette (Fig. 2). In the case of the outside-out patch clamp recordings performed to gather single-channel I-V data, a fast solution exchange was not required, and hence, the recording compartment was perfused manually. All other recordings were performed in the cell-attached configuration. Both macroscopic and single-channel currents were recorded using an Axopatch 200B amplifier (MDS Analytical Technologies) at room temperature (~22°C) and were digitized at 100 kHz. Series resistance compensation was used and set to 70–80% during all macroscopic recordings. The effective bandwidth before data analysis was DC–5 kHz for macroscopic currents and DC–20 kHz for single-channel currents. During the experiments aimed at characterizing the Ca^{2+} currents through mutant and wild-type receptors, different voltages were applied to cell-attached or outside-out patches to generate single-channel I-V curves. During all other experiments, the applied potential was fixed at −80 mV (negative inside the cell).

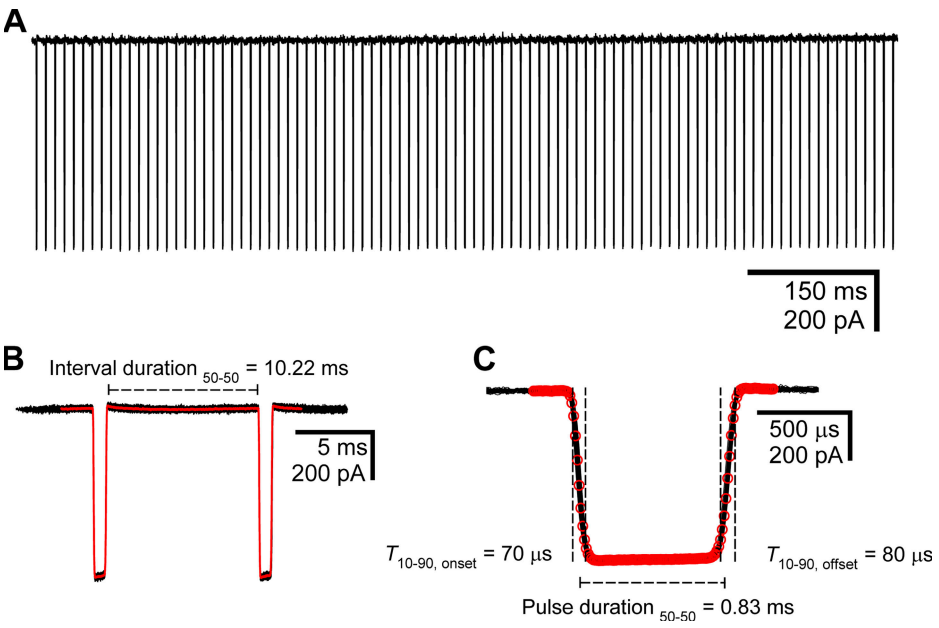

Figure 2. Calibration of the solution-switching system. The different parameters of the solution-switching system (that is, diameter of the theta tube openings, relative positioning of the theta tube and patch pipette, rate of solution flow, and bandwidth of the computer-generated waveform) were adjusted so as to optimize the time course of the solution exchange. The latter was estimated by measuring the liquid-junction potential by alternatively exposing the tip of an open pipette (containing 150 mM K-aspartate and 20 mM KCl) to 1 M KCl (for 0.8 ms) and 150 mM KCl (for 10 ms) solutions. (A) Representative train of 93 pulses of 1 M KCl delivered at ~100 Hz. (B) The train in A was segmented into two-pulse segments, and these were aligned and averaged (red trace). (C) The first half of the traces in B is magnified to emphasize the rise time during the onset and the offset, as well as the duration of each pulse.

Solutions

In the case of the concentration-jump experiments, the solution flowing through both barrels of the theta tube and through the gravity-fed perfusion contained the following (in mM): 142 KCl, 5.4 NaCl, 1.8 $CaCl_2$, 1.7 $MgCl_2$, and 10 HEPES/KOH, pH 7.4. In addition, the solution flowing through one of the theta tube barrels also contained ACh (1 mM in the case of the severe loss-of-function εP121L mutant and 100 μM in all other cases). The pipette solution was either the same KCl-based solution used to perfuse the patches or a KF, low divalent cation solution consisting of the following (in mM): 100 KF, 40 KCl, 1 $CaCl_2$, 11 EGTA, and 10 HEPES/KOH, pH 7.4; this KF-based solution improved the stability of the membrane patches. In the case of the outside-out current recordings aimed at obtaining data for single-AChR I-V relationships, both the pipette solution and that bathing the external aspect of the patches consisted of the following (in mM): 150 NaCl, 1.7 $MgCl_2$, 10 HEPES/KOH, pH 7.4, and the indicated concentration of Ca^{2+} added as $CaCl_2$. This NaCl-based solution with variable $CaCl_2$ was also used in the pipette during the recording of single-AChR I-V data in the cell-attached configuration. All I-V data from the AChR were recorded in the presence of 1 μM of extracellular ACh either in the pipette or the bath, depending on the configuration. Single-channel I-V data from the NMDAR were recorded in the cell-attached configuration using a nominally Mg^{2+}-free pipette solution consisting of the following (in mM): 150 NaCl, 0.1 glutamate, 0.1 glycine, 10 HEPES/KOH, pH 7.4, and the indicated concentration of Ca^{2+} added as $CaCl_2$. Osmolarity differences arising from the variable Ca^{2+} concentrations were not compensated. During recordings in the cell-attached configuration, the cells were bathed in a depolarizing KCl solution consisting of the following (in mM): 142 KCl, 5.4 NaCl, 1.8 $CaCl_2$, 1.7 $MgCl_2$, and 10 HEPES/KOH, pH 7.4. During outside-out experiments, the cells were bathed in an "extracellular-like" NaCl solution consisting of the following (in mM): 137 NaCl, 2.7 KCl, 0.9 $CaCl_2$, 0.5 $MgCl_2$, 8 Na_2HPO_4, and 1.5 mM KH_2PO_4, titrated to pH 7.3 with HCl.

Data Analysis

Macroscopic currents in response to step changes in the concentration of ACh were analyzed using a combination of pClamp 9.0 (MDS Analytical Technologies), SigmaPlot 7.101 (SPSS Inc.), and in-house–developed programs, whereas single-channel currents were analyzed using the SKM option in QuB software (Qin et al., 1996; Qin, 2004; http://www.qub.buffalo.edu) and SigmaPlot 7.101 (SPSS Inc.).

The kinetics of ACh-elicited currents through the muscle AChR were analyzed in the framework of the reaction scheme shown in Fig. 1, according to which the transmitter-binding sites can be unliganded, monoliganded, or diliganded, and the conformation of the channel can be closed, open, or desensitized. For simplicity, only one of the (probably several) desensitized conformations is included in the model. Also, the two neurotransmitter-binding sites are assumed to be functionally equivalent and, therefore, the two possible monoliganded configurations are considered to be functionally indistinguishable. These simplifications have no consequences on the interpretation of our data.

The time constant of the macroscopic-current decay upon stepping the concentration of ACh from saturating to zero (that is, during channel deactivation) coincides with the mean duration of a burst of single-channel fully liganded openings (Colquhoun et al., 1997; Wyllie et al., 1998). According to Fig. 1, such a "burst" consists of several consecutive $CA_2 \rightleftharpoons OA_2$ interconversions terminated by ACh dissociation or entry into desensitization. Hence, the mean duration of a burst is largely determined by the rate constants of diliganded channel gating, agonist dissociation (from CA_2 or OA_2), and entry into desensitization (from CA_2 or OA_2). In the muscle AChR, ACh dissociation proceeds mainly from CA_2, but some dissociation from OA_2 cannot be completely ruled out (Grosman and Auerbach, 2001). Similarly, experimental data strongly suggest that entry into desensitization can proceed from OA_2 (Auerbach and Akk, 1998; Elenes et al., 2006), but whether it cannot proceed at all from CA_2 is more difficult to ascertain. Throughout the rest of this paper, we assume that desensitization of diliganded AChRs can only occur from OA_2, for simplicity. It is clear, from our earlier work, that the increased contribution of entry into desensitization to deactivation observed for mutants with increased diliganded-gating equilibrium constant corresponds to desensitization arising from OA_2, but we cannot rule out that these receptors also desensitize from CA_2, at least to some degree. Again, this simplification has no consequences whatsoever on the conclusions of this work. Thus, neglecting entry into desensitization from CA_2, and taking into account that, in the cases of the wild-type and gain-of-function mutant AChRs studied here, most of the length of a burst is spent in the open state, the mathematical expression for the deactivation time constant is given by (Elenes et al., 2006):

$$\tau_{\text{deactivation}} \cong \frac{1}{D_+ + 2j_- + \dfrac{\alpha_2 2k_-}{\beta_2 + 2k_-}}, \qquad (1)$$

where the symbols are defined in Fig. 1, and where the probability of a burst of single-channel diliganded openings being terminated by entry into desensitization, rather than by agonist dissociation, is given by the product of D_+ and $\tau_{\text{deactivation}}$. Hence, the slower the deactivation time course, the larger the contribution of desensitization to the termination of a burst. Adult mouse muscle wild-type values for the rate constants in Eq. 1 are $\beta_2 \cong 50{,}000\ s^{-1}$, $\alpha_2 \cong 2{,}000\ s^{-1}$, $2k_- \cong 50{,}000\ s^{-1}$, $2j_- < 10\ s^{-1}$, and $D_+ \cong 25\ s^{-1}$. Therefore, in the case of the adult wild-type AChR (but, clearly, not in the case of gain-of-function mutants), Eq. 1 may be considered to reduce to $\left[\left(1+\beta_2/2k_-\right)/\alpha_2\right]$, the more familiar expression of Colquhoun and Hawkes (1982).

Experimentally, the kinetics of deactivation were estimated by exposing outside-out patches to low-frequency trains of ~0.8-ms pulses of ACh (1 mM for εP121L and 100 μM for all other constructs) at −80 mV. All traces within a train were aligned and averaged, and the decaying phase was fitted (least-squares method) from the peak of the current until the end of the transient with a mono-exponential function (Table I). The frequency of such trains varied among constructs and was chosen so as to minimize the fading of the response.

The kinetics of entry into desensitization were estimated by exposing outside-out patches to ~2-s pulses of 1 mM (εP121L) or 100 μM ACh (all other constructs) at −80 mV. The decaying phase of these current transients were fitted (least-squares method) from the peak of the currents until the end of the 2-s ACh applications with one or two exponential components. The parameters of these exponential fits were used to calculate "desensitization half-times"; this is the way in which the kinetics of entry into desensitization are expressed in Table I. The use of these phenomenological "half-times" was necessary because we needed to somehow compare the time courses of desensitization of the analyzed constructs. And although the wild-type AChR and some of the slow-channel mutants desensitize following a mono-exponential time course, others do so with double-exponential kinetics (this was also the case for the set of gain-of-function mutations at the δM2 12′ position studied by us previously; Elenes et al., 2006). Of course, when a time course is best described by a double-exponential function, nothing exact can be done to compare it with the kinetics of a mono-exponential time course. We found, however, that the half-decay times calculated from the

TABLE I

Kinetic Parameters of a Set of Wild-type AChRs and Naturally Occurring Mutants

Construct	$\tau_{deactivation}$ (ms)[a]	$t_{1/2,\ desensitization}$ (ms)[b]	Paired-pulse $\tau_{recovery}$ (ms)[c]	Train $\tau_{recovery}$ (ms)[d]
εP121L (adult, mouse)	0.37 ± 0.02 (7)	66 ± 10 (9)	101 ± 18 (6)	ND[e]
δD59K (adult, mouse)	0.92 ± 0.08 (10)	38 ± 7 (7)	71 ± 5 (3)	ND
wild-type/ε (adult, mouse)	0.98 ± 0.06 (25)	22 ± 3 (13)	306 ± 19 (5)	500 (6)
wild-type/γ (fetal, mouse)	4.5 ± 0.5 (10)	31 ± 12 (3)	290 ± 33 (4)	167 (4)
βV266M (adult, mouse)	5.4 ± 0.1 (10)	38 ± 6 (4)	279 ± 26 (2)	167 (4)
εL221F (adult, mouse)	6.6 ± 0.4 (17)	34 ± 12 (4)	466 ± 21 (4)	1,333 (8)
αS269I (adult, mouse)	9.2 ± 0.7 (10)	20 ± 4 (9)	552 ± 29 (5)	667 (4)
εL269F (adult, mouse)	19 ± 2 (11)	28 ± 5 (10)	1,830 ± 170 (5)	1,000 (7)
εT264P (adult, mouse)	21 ± 1 (29)	99 ± 10 (11)	742 ± 37 (2)	1,000 (8)

[a]Deactivation time constants estimated from mono-exponential fits. The numbers in parentheses indicate the number of low-frequency trains of 0.8-ms ACh pulses analyzed. Each train consisted of at least 10 pulses, the responses to which were averaged and fitted. Average values across trains are given as mean ± SE.

[b]Desensitization half-times. In some cases, the time course of entry into desensitization was best fitted with two, rather than one, exponential components. Hence, to facilitate the comparison, the parameters of these fits (whether single or double exponential) were used to numerically solve for the corresponding desensitization half-times (that is, the time taken for the current decay to be half-complete). The numbers in parentheses indicate the number of analyzed responses. Average values are given as mean ± SE.

[c]Recovery from desensitization time constants estimated from the response to paired-pulse protocols. The numbers in parentheses indicate the number of independent experiments analyzed to generate the plots in Fig. 3 C.

[d]Recovery from desensitization time constants estimated from the fitting of the plots in Fig. 5 as described in Materials and methods. The best-fit values were identified by manually adjusting the unknown parameter, and standard errors were not estimated.

[e]Not determined. This parameter was estimated only for wild-type and slow-channel mutant AChRs.

parameters of the double-exponential fits provide an excellent approximation to the desensitization time course during the first tens of milliseconds. In other words, when we plot the experimentally obtained double-exponential desensitization decays and the mono-exponential decays calculated from the respective $t_{1/2}$ values ($t_{1/2}/ln2$, more precisely), we find a very close agreement between both curves during the first tens of milliseconds. After these initial milliseconds, the time courses deviate from one another, but it is these initial tens of milliseconds that matter in the context of the 50-Hz trains (that is, 20-ms interpulse intervals) applied here. Hence, mono- and double-exponential desensitization time courses are compared using their corresponding half-times. A double-exponential time course of entry into desensitization with a near-zero current at equilibrium suggests the existence of, at least, two desensitized conformations of different stability. On average, in the sustained presence of a high concentration of ACh, the least stable desensitized state would be visited several times by an actively opening and closing AChR before the more stable desensitized conformation is finally reached.

The kinetics of recovery from desensitization were estimated using pairs of conditioning and test pulses (1 s and 100 ms in duration, respectively) of 1 mM (εP121L) or 100 μM ACh (all other constructs), separated by ACh-free intervals of variable length, at −80 mV. Because desensitization was nearly complete at the end of each conditioning pulse, the fraction of recovered AChRs could be well approximated by the ratio between the peak-current elicited by the test pulse and that elicited by the conditioning pulse in each pair. The interval between any two consecutive pairs of pulses was ≥10 s to ensure complete recovery from desensitization. Plots of recovered fraction of receptors as a function of the duration of the interpulse interval were well fitted with mono-exponential rise functions ($\text{Recovered fraction} = 1 - \exp(-t/\tau)$) despite the multiple steps that must be involved in the recovery of ACh-diliganded desensitized receptors after ACh removal. The time constants corresponding to the different AChR constructs studied here are listed in Table I. It could be argued, however, that the kinetics of recovery from the desensitized state(s) reached upon exposure of the AChR to high concentrations of ACh for 1 s may not be representative of the kinetics of recovery that are relevant during application of trains of ∼0.8-ms pulses of ACh. Indeed, it has been reported that the longer the exposure to high concentrations of ACh, the slower the kinetics of recovery on removal of the agonist (Reitstetter et al., 1999), as if a prolonged interaction of the desensitized receptor with ACh favored the transition to increasingly more stable desensitized conformations. To address this issue, we applied a second method to estimate the kinetics of recovery. This method is based on the notion that the response of the AChR to trains of brief pulses of saturating ACh can be kinetically modeled using a cyclic three-state scheme in which several of the states shown in Fig. 1 are conveniently grouped (Elenes et al., 2006). According to this "triangular" model, during the brief (<1-ms) pulses of saturating ACh, the AChR dwells in "activated states" (CA_2 and OA_2) and, upon ACh washout, the receptor relaxes to either "activatable" (CA and C) or desensitized states (DA_2, DA, and D). During the ACh-free interpulse intervals, the desensitized AChR can lose the bound ACh and close ("recover"), thus joining the pool of activatable receptors. Finally, we assume that all of the AChRs that are in activatable states by the end of each interpulse interval are converted into activated AChRs on application of the following pulse of saturating

ACh, an assumption that follows from the known kinetic properties of the wild-type and mutant AChRs tested here. In the framework of this model, the rates at which the activated states relax into activatable or desensitized states can be calculated from the experimentally estimated time constants of deactivation and desensitization; the only unknown kinetic parameter, then, is the rate of recovery during the interpulse intervals. The mathematical expression for the fraction of receptors in activated states at the beginning of each ACh pulse was derived analytically (using the three-state kinetic scheme), and the rate of recovery of each construct was adjusted manually until a satisfactory fit (as judged by eye) to the experimental data shown in Fig. 5 was reached. These recovery rates, expressed as their reciprocals, are presented in Table I for comparison with the recovery time constants estimated from paired-pulse experiments. More details as to the methodological aspects of this approach are presented in Elenes et al. (2006).

RESULTS

Slow-Channel Syndrome Mutants Desensitize upon ACh Removal

Application of high-frequency trains of brief ACh pulses to wild-type and laboratory-engineered gain-of-function mutant receptors (a series of single–amino acid replacements at the 12′ position of the pore-lining M2 segment of the δ subunit) confirmed the notion that the AChR can desensitize upon agonist removal (Elenes et al., 2006). As expected from all we know about this receptor channel (for example, Edmonds et al., 1995), the extent of desensitization during deactivation was found to be small in the wild type. However, as can be predicted from Fig. 1 and Eq. 1, this depression became more profound as the deactivation time constant was increasingly prolonged by mutations. It should be noted here that the duration of the ACh pulses (~0.8 ms) is too short for desensitization to be appreciable within each pulse. Instead, virtually all of the desensitization takes place after removing the agonist, as one of the pathways for burst termination, during the much longer interpulse intervals.

Slow-channel syndrome mutants also deactivate more slowly than the wild type (Engel et al., 2003), and thus, could also be thought to desensitize appreciably on agonist removal. However, as mentioned above, generalizations as to the extent of desensitization within a high-frequency train of ACh pulses cannot be made solely on the basis of deactivation time-constant values (or, equivalently, single-channel mean burst durations) because mutations may affect the kinetics of desensitization as well. Hence, the kinetics of desensitization and/or the response to repetitive applications of agonist need to be studied for each individual mutant.

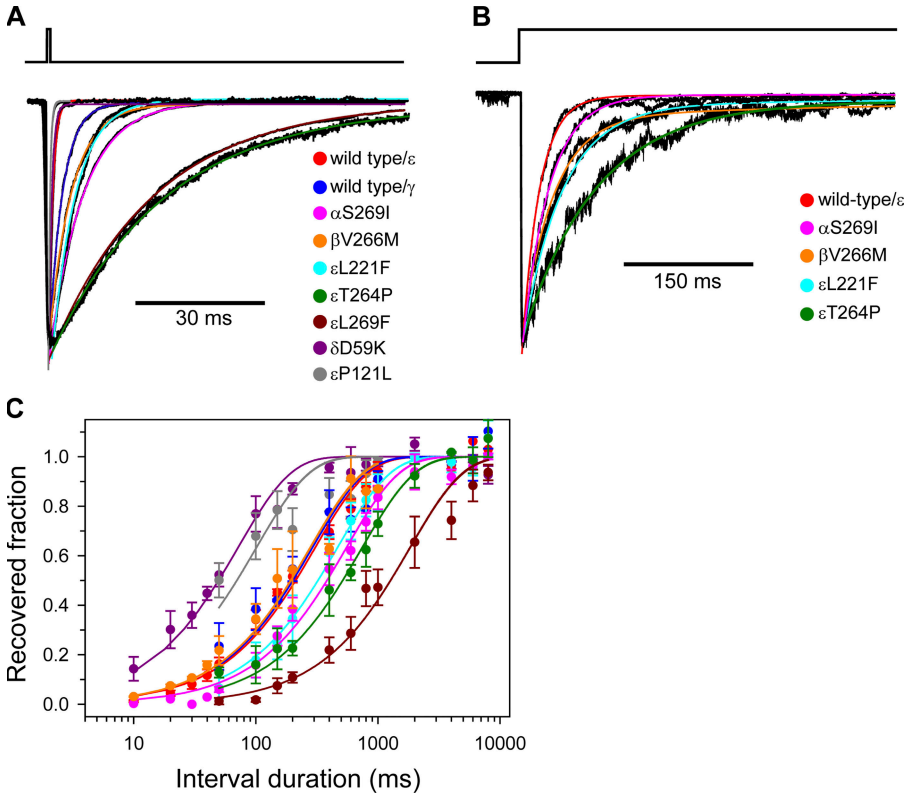

Figure 3. Kinetics of mouse muscle AChR deactivation, entry into desensitization, and recovery from desensitization. (A) Kinetics of deactivation. Each plotted trace is the average response of a patch to several 0.8-ms pulses of ACh (100 such pulses for εP121L, 5 for εL269F, and 10 for all other constructs) applied as low-frequency trains. The deactivation time constants, estimated from mono-exponential fits to the decaying phase of these plots, were in turn averaged over several such trains and are listed in Table I. (B) Kinetics of entry into desensitization. For clarity, only the responses of some of the studied constructs to the 2-s pulses of ACh are shown. Only the first 450 ms of these responses are displayed. The parameters estimated from the exponential fits to the decaying phase of these time courses were used to calculate desensitization half-times (see Materials and methods). The corresponding averages, over several responses per construct, are listed in Table I. (C) Kinetics of recovery from desensitization estimated using pairs of conditioning (1-s) and test (100-ms) pulses of ACh. The color key is the same as in A. Vertical error bars are standard errors calculated from the results of several independent experiments. The time constants of mono-exponential rise fits to the plots of recovered fraction as a function of the duration of the interpulse intervals (see Materials and methods) are listed in Table I. The concentration of ACh applied during the pulses, in all three panels, was 1 mM in the case of the severe loss-of-function εP121L mutant and 100 μM in all other cases.

We set out to investigate a panel of five slow-channel mutations in different subunits and regions of the AChR: αS269I (Croxen et al., 1997), in the linker between the M2 and M3 transmembrane segments; βV266M (Engel et al., 1996), in M2; εL221F (Croxen et al., 2002; Hatton et al., 2003), in the linker between β-strand 10 and M1; εT264P (Ohno et al., 1995), in M2; and εL269F (Gomez and Gammack, 1995; Engel et al., 1996), also in M2. As a negative control, we also studied two naturally occurring mutants with faster kinetics of deactivation (and which cause another variant of the congenital myasthenic syndrome known as "fast-channel syndrome"). These were δD59K (δE59K, in humans; Brownlow et al., 2001), close to loop D of the N-terminal extracellular domain, and εP121L (Ohno et al., 1996), near the cysteine loop.

Fig. 3 shows the response of multichannel outside-out patches to brief pulses (Fig. 3 A), long pulses (Fig. 3 B), and pairs of conditioning and test pulses of ACh (Fig. 3 C). Analysis of these data yielded time constants of deactivation, entry into desensitization, and recovery from desensitization, respectively (Table I). Fig. 4 shows some representative responses to trains of ACh pulses delivered at a frequency of 50 Hz (a physiologically relevant frequency in the context of the neuromuscular junction; Hennig and Lømo, 1985), and Fig. 5 shows their normalized peak-current values, averaged over several experiments. Inspection of the kinetic parameters in Table I reveals that it is mostly the kinetics of deactivation that are affected by these naturally occurring mutations. The kinetics of entry into and recovery from desensitization are affected to a lesser extent, and in some cases, these changes would even accentuate the depression (such as the slower recovery from desensitization of some of the mutants). Thus, the response to successive applications of ACh decreases along the trains (Figs. 4 and 5), with the degree of depression roughly mirroring the constructs' deactivation time constants, exactly as expected from a channel that can desensitize from the open-diliganded conformation. Indeed, the two faster than wild-type mutants, δD59K and εP121L (Table I), display very little (εP121L), if any (δD59K), depression. Notably, the deactivation time constant of the εT264P mutant is so much longer than the wild type's (a factor of ∼20) that, even though its entry into desensitization rate is slower by a factor of ∼4, the response to a 50-Hz train of ACh pulses still decreases markedly.

The recovery time constants estimated using a classical two-pulse protocol with a 1-s conditioning pulse (Fig. 3 C) could well be irrelevant if it is the kinetics of recovery during the repetitive (50 Hz) application of <1-ms pulses that matter. To clarify this point, we fitted the data in Fig. 5 with a simplified kinetic scheme that

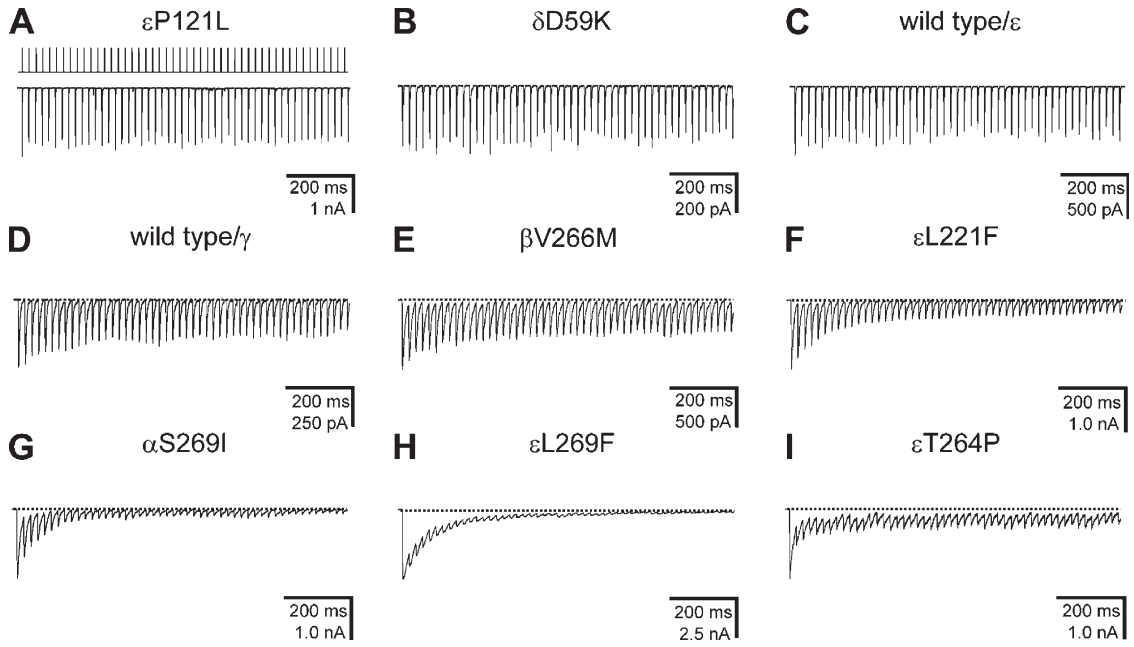

Figure 4. Slow-channel syndrome AChRs desensitize during deactivation. (A–I) Example current traces recorded from individual outside-out patches. Each panel shows the response of a different mouse muscle AChR construct to the application of a 50-Hz train of 0.8-ms ACh pulses (1 mM in A and 100 μM in B–I). One such train is indicated in A above the current trace. The zero-current level is indicated, on each trace, with a dotted line. The plots are presented in increasing order of deactivation time constant (Table I). The prediction (made on the basis of the kinetic scheme in Fig. 1 and Eq. 1) that the slower the deactivation time course the more pronounced the depression is borne out by these recordings. Of course, because the kinetics of entry into and recovery from desensitization are not completely unaffected by the mutations (Table I), this relationship cannot be perfect. However, the trend is undoubtedly clear (see also Fig. 5).

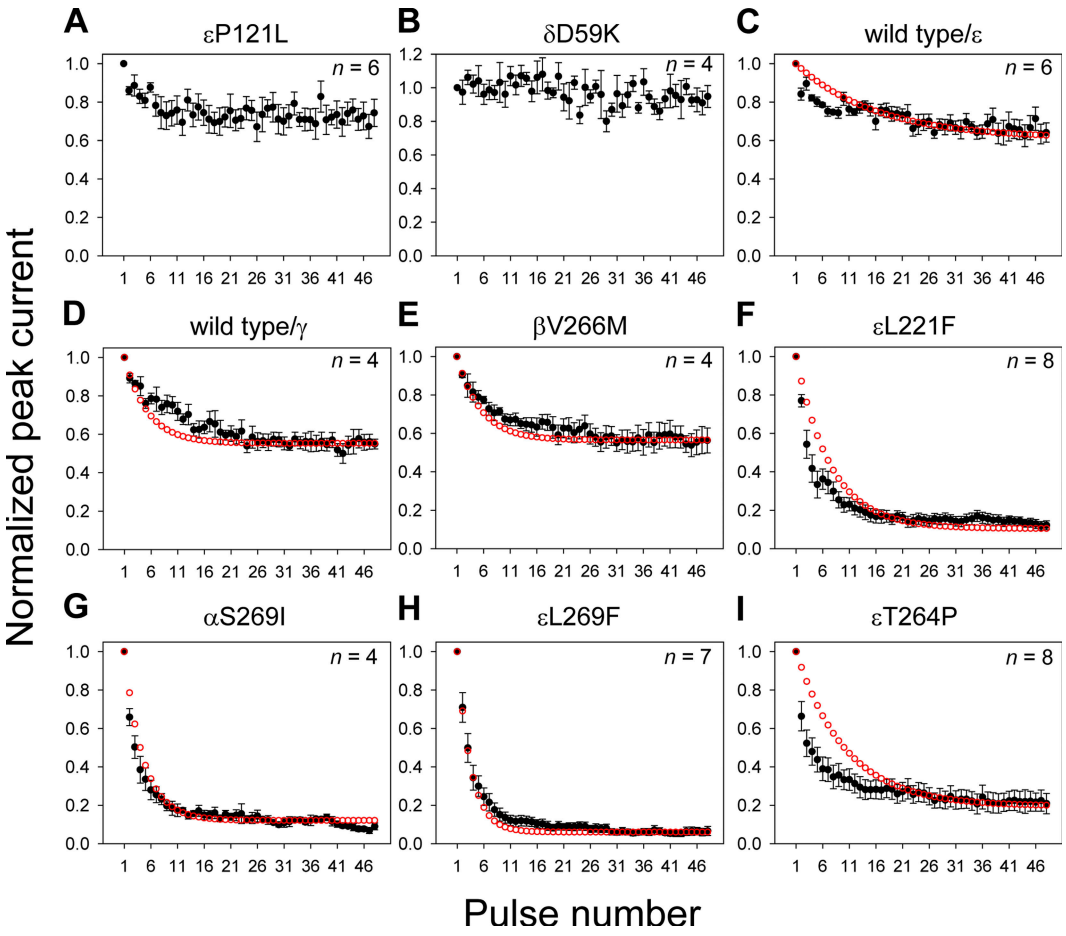

Figure 5. Depression of ACh-evoked currents upon repetitive stimulation. (A–I) Peak-current values in response to 50-Hz trains of 0.8-ms ACh pulses were normalized with respect to the first peak in each series and averaged across replicate experiments. The number of averaged responses (*n*) is indicated for each construct. Vertical error bars are standard errors. Example current traces are given in Fig. 4. The red circles correspond to the fits from which estimates of the rate of recovery from desensitization within a train of ACh pulses were obtained (see Materials and methods). These values are expressed as time constants in Table I. These fits were performed only for the wild-type and gain-of-function mutant AChRs.

groups all possible states of the AChR in Fig. 1 into activated (CA_2 and OA_2), activatable (CA and C), and desensitized classes (DA_2, DA, and D; see Materials and methods). Evidently (everything else being equal), the slower the kinetics of recovery, the more pronounced the decline of the current response. The fits are shown in Fig. 5 and the estimated recovery time constants are listed in Table I for comparison to those obtained from paired-pulse experiments. On the one hand, inspection of these values reinforces the notion that the kinetics of recovery from desensitization change much less upon mutation than those governing deactivation. On the other hand, the fact that these two types of "recovery time constants" differ numerically so little from each other is surprising, especially considering that, in one case, the desensitized conformation(s) is (are) reached under the continuous presence of ACh (during the 1-s conditioning pulses), whereas, in the other case, desensitization takes place during the ACh-free, 20-ms interpulse intervals. It is likely that incubations with ACh longer than 1 s are needed for this channel to attain the more reluctant to recover desensitized conformations that have been reported for the muscle AChR (Reitstetter et al., 1999).

As a further control for these experiments, we exposed two of the slow-channel mutants (εL221F and εT264P) to trains of ACh pulses delivered at different frequencies, from 2.5 to 100 Hz (Fig. 6). Reassuringly, the recordings show that the higher the frequency, the deeper the steady-state depression, exactly as expected if this progressive attenuation of the currents were due to the accumulation of channels in the desensitized state. Finally, in an attempt to mimic the heterozygous state of mutations, we cotransfected HEK-293 cells with wild-type and L269F ε-subunit cDNAs in equimolar proportions (in addition to α1-, β1-, and δ-subunit cDNAs). As could be anticipated if the two alternative constructs expressed with the same efficiency, the response of the "heterozygous patches" is almost exactly halfway between those of patches expressing only wild-type or only L269F ε-subunits (Fig. 7; see also Fig. 5).

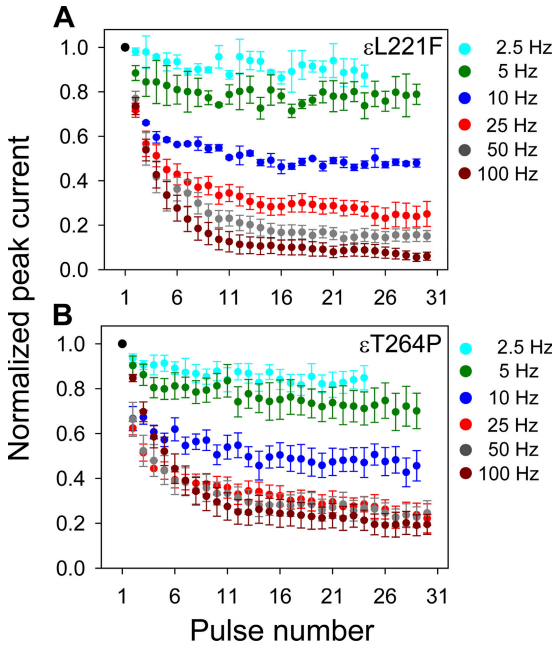

Figure 6. Frequency dependence of the AChR response to trains of ACh pulses. (A and B) Normalized current responses of two slow-channel syndrome mutants to trains of 0.8-ms pulses of 100 µM ACh delivered at different frequencies. The responses to several trains at each frequency were averaged. Vertical error bars are standard errors. In A, the number of averaged trains was 3 at 2.5, 5 and 10 Hz, 10 at 25 Hz, and 8 at 50 and 100 Hz. In B, the number of averaged trains was 6 at 2.5 and 10 Hz, 5 at 5 Hz, 14 at 25 Hz, 8 at 50 Hz, and 7 at 100 Hz. The y-axis value corresponding to the first pulse in each train (black symbol) is the same for all trains.

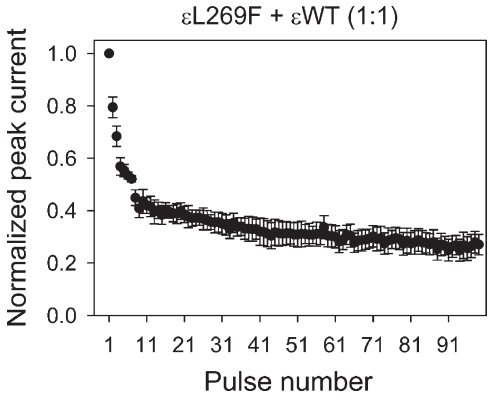

Figure 7. Mimicking the heterozygous state of a slow-channel mutation. Normalized current responses of outside-out patches excised from cells expressing a mixture of both wild-type and L269F ε-subunits (along with all other mouse muscle AChR wild-type subunits) to trains of 0.8-ms pulses of 100 µM ACh delivered at 50 Hz. In these experiments, each train consisted of 100 pulses. Vertical error bars are standard errors. The responses to five trains were averaged.

Because the slow-channel mutations studied here were engineered on the corresponding mouse AChR cDNA clones, it seemed prudent to validate this approach by analyzing the behavior of the human receptor. Fig. 8 compares the kinetics of deactivation, entry into desensitization, and recovery from desensitization of these two muscle- and adult-type AChRs. For the human receptor: $\tau_{deactivation}$ = (1.3 ± 0.06) ms (n = 16 trains); $t_{1/2,\ desensitization}$ = (16 ± 2) ms (n = 10 pulses); and paired-pulse $\tau_{recovery}$ = (397 ± 28) ms (data from six patches). We also compared the responses to trains of ACh pulses delivered at 50 Hz (Fig. 9); for the human receptor, train $\tau_{recovery}$ = 385 ms (n = 7 trains). The close agreement between the values of these kinetic parameters in humans and mice (Table I) amply justifies our use of the mouse clones to elucidate the molecular basis of this human condition. Of particular interest, note that under the repetitive exposure to ACh illustrated in Fig. 9, only ~50% of the human receptors remain activatable after ~25 pulses; the response of the mouse AChR depresses less deeply, with ~65% of the receptors remaining activatable after ~25 pulses. The somewhat slower deactivation time course and faster entry into desensitization of the human counterpart can account for the observed increased attenuation of the currents.

Slow-Channel Mutants Conduct Ca^{2+} as Fast as the Wild-type AChR

Although the molecular determinants of cation versus anion selectivity in the AChR's (and all other Cys-loop receptors') permeation pathway are limited quite narrowly to only a few positions on the cytoplasmic end of the pore-lining M2 segments (Galzi et al., 1992; Corringer et al., 1999), the determinants of Ca^{2+} conduction have been reported to be scattered along, and even outside, the pore domain (for example, Bertrand et al., 1993). Hence, the suggestion that some slow-channel mutants display an increased Ca^{2+} permeability, and that this increased permeability intensifies the Ca^{2+} overload of the motor endplate (Di Castro et al., 2007), seems plausible and worth investigating.

When it comes to characterizing the relative permeability of Ca^{2+} through an ion channel in a physiological context, the concept of fractional Ca^{2+} currents (that is, the fraction of the total current that is carried by Ca^{2+} under physiological membrane potential and ion conditions) seems far more appropriate than the use of permeability ratios calculated from reversal potentials using the Goldman-Hodgkin-Katz voltage equation. Fractional Ca^{2+} currents have been typically estimated from the combined application of whole cell current recordings and Ca^{2+}-influx measurements using Ca^{2+} chelators that change their fluorescent properties upon complex formation (Thayer et al., 1988; Neher and Augustine, 1992; Zhou and Neher, 1993; Vernino et al., 1994). The accurate estimation of Ca^{2+} influx, however, is not straightforward. On the one hand, the cytosolic concentration of Ca^{2+} is not only determined by its influx through the channel under study, but it also depends on the activity of cellular Ca^{2+}-buffering systems and other Ca^{2+}-transport membrane proteins. On the other hand, the entry of Ca^{2+} into the cell can elicit

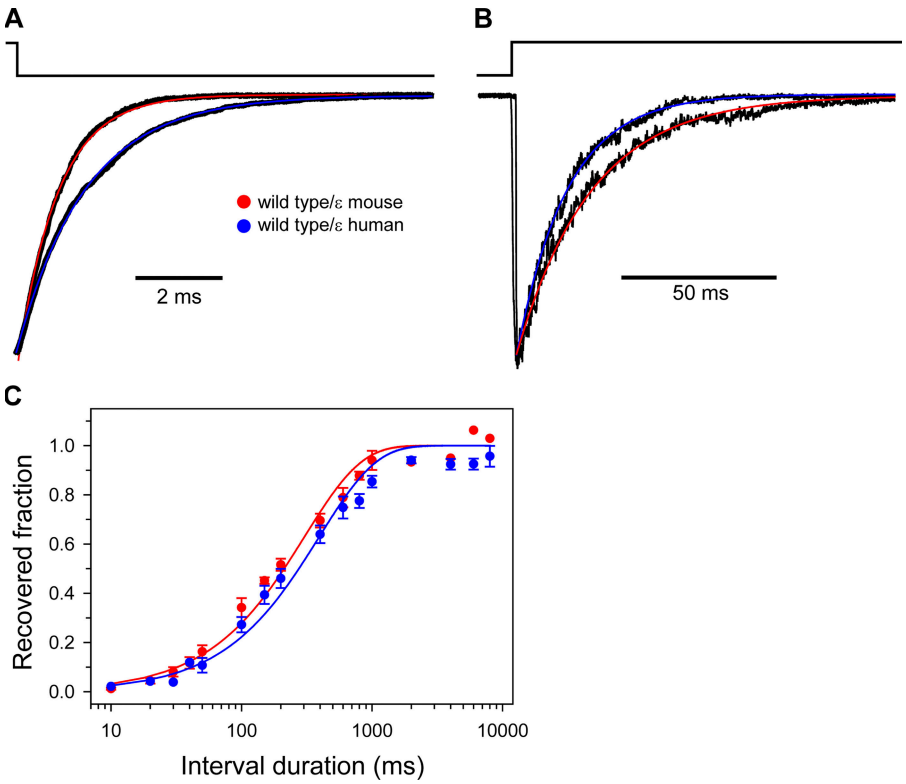

Figure 8. Comparison of the kinetics of AChR deactivation, entry into desensitization, and recovery from desensitization in human and mouse muscle wild-type AChRs. (A) Kinetics of deactivation. Each plotted trace is the average response of a patch to 10 0.8-ms pulses of 100 μM ACh applied as low-frequency trains. Only the decaying phase is displayed to emphasize the slower decay time course of the human receptor. (B) Kinetics of entry into desensitization. Only the first ~125 ms of these responses to 100 μM ACh are displayed. The color key is the same as in A. (C) Kinetics of recovery from desensitization estimated using pairs of conditioning (1-s) and test (100-ms) pulses of 100 μM ACh. Vertical error bars are standard errors calculated from the results of several independent experiments. The color key is the same as in A. All kinetic parameters were estimated as indicated in Materials and methods.

Ca^{2+}-activated conductances that may contribute undesired currents to the whole cell recordings. Finally, the specific calibration approach followed to transform the units of fluorescence into values of Ca^{2+} influx seems to be an added source of discrepancy among the values of fractional Ca^{2+} currents reported in the literature (Rogers and Dani, 1995; Schneggenburger, 1996).

Given this scenario, we decided to apply an alternative method to estimate the magnitude of the Ca^{2+} currents through the muscle AChR heterologously expressed in HEK-293 cells. Our approach consisted of the measurement of single-channel I-V curves in the cell-attached configuration with a physiological concentration of Na^+ and Mg^{2+} in the pipette (that is, the extracellular side) and with varying concentrations of Ca^{2+} (from nominally zero to saturating). A simultaneous fit of all the I-V data with a model that assumes that K^+ (from the cytosol), Na^+, Mg^{2+}, and Ca^{2+} compete for a single site in the permeation pathway yields estimates of the three unknown parameters, namely, the single-channel conductance in the absence of Ca^{2+} ($\gamma_{Na^+\text{-}Mg^{2+}}$; we name this parameter after the predominant current carriers at the assayed hyperpolarized potentials), the single-channel conductance in the presence of saturating Ca^{2+} ($\gamma_{Ca^{2+}}$), and the (reciprocal of the) apparent affinity of Ca^{2+} for the site in the channel's pore in the presence of physiological concentrations of Na^+ and Mg^{2+} ($K_{D_{Ca^{2+}}}$). From these values, the composition of the total current (i_{total}) in terms of the amount carried by the Na^+–Mg^{2+} mixture ($i_{Na^+\text{-}Mg^{2+}}$) and the amount carried by Ca^{2+} ($i_{Ca^{2+}}$) can be calculated at any (hyperpolarized) membrane potential (V) and extracellular Ca^{2+} activity ($a_{Ca_o^{2+}}$). From this composition, in turn, the fraction of the total current carried by Ca^{2+} can, also, be easily obtained. Because we used a saturating concentration of Na^+ in the pipette solution (150 mM; Fig. 10), the probability of the pore's cation-binding site being occupied was near unity at all values of $[Ca^{2+}]_o$ and voltages. Under these conditions, the equations take the following trivial forms:

$$i_{total} = i_{Na^+\text{-}Mg^{2+}} + i_{Ca^{2+}} \tag{2}$$

$$i_{Na^+\text{-}Mg^{2+}} = \gamma_{Na^+\text{-}Mg^{2+}} \frac{K_{D_{Ca^{2+}}}}{K_{D_{Ca^{2+}}} + a_{Ca_o^{2+}}} V \tag{3}$$

$$i_{Ca^{2+}} = \gamma_{Ca^{2+}} \frac{a_{Ca_o^{2+}}}{K_{D_{Ca^{2+}}} + a_{Ca_o^{2+}}} V \tag{4}$$

and

$$\text{Fractional } Ca^{2+}\text{current} = \frac{i_{Ca^{2+}}}{i_{total}} = \frac{\gamma_{Ca^{2+}}\ a_{Ca_o^{2+}}}{\gamma_{Ca^{2+}}\ a_{Ca_o^{2+}} + \gamma_{Na^+\text{-}Mg^{2+}}\ K_{D_{Ca^{2+}}}}, \tag{5}$$

where the ratios $a_{Ca^{2+}}/(K_{D_{Ca^{2+}}}+a_{Ca^{2+}})$ and $K_{D_{Ca^{2+}}}/(K_{D_{Ca^{2+}}}+a_{Ca^{2+}})$ give the probabilities of the (phenomenologically defined) cation-binding site in

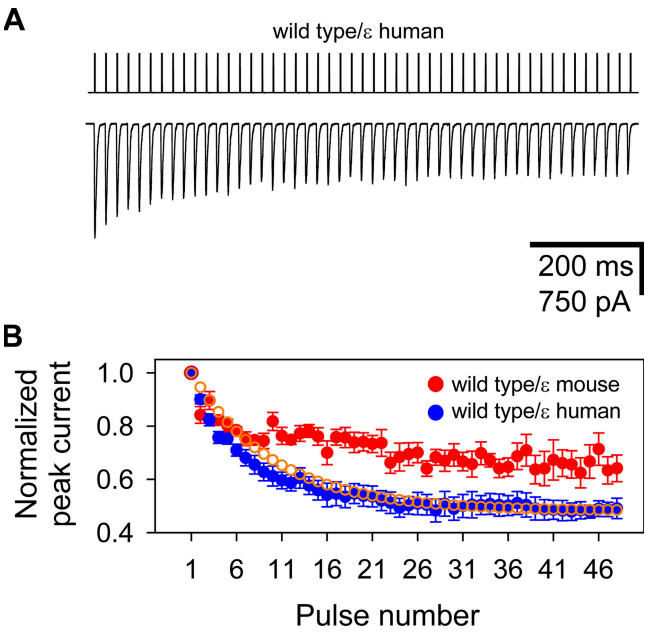

Figure 9. Depression of ACh-evoked currents through human and mouse muscle wild-type AChRs. (A) Example current trace recorded from an outside-out patch containing human muscle wild-type AChRs exposed to a 50-Hz train of 0.8-ms ACh pulses (100 μM). The train of pulses is indicated above the current recording. (B) Peak-current values in response to the applied 50-Hz trains were normalized with respect to the first peak in each series and averaged across replicate experiments (six for the mouse AChR and seven for the human counterpart). Vertical error bars are standard errors. The orange circles superimposed on the human AChR data points correspond to the fit from which the estimate of the rate of recovery from desensitization within a train of ACh pulses was obtained (see Materials and methods). The corresponding fit to the mouse AChR data points is shown in Fig. 5.

the pore being occupied by Ca^{2+} or by a permeant cation other than Ca^{2+}, respectively. Further, the extracellular Ca^{2+} activity ($a_{Ca_o^{2+}}$) was calculated as the product of the extracellular molarity of calcium ions ($[Ca^{2+}]_o$, which is very close to the corresponding molality, for the solutions we used here) and the square of the mean activity coefficient of $CaCl_2$ in the presence of 150 mM NaCl, following the work of Butler (1968) and using values tabulated in Robinson and Stokes (1955).

Fig. 11 shows I-V data, recorded in the cell-attached configuration, for the slow-channel mutants studied in the previous section of this paper and for several wild-type AChRs. Fig. 12 shows some representative single-channel traces, and Table II shows the fitted values of $\gamma_{Ca^{2+}}$, $\gamma_{Na^+\text{-}Mg^{2+}}$, and $K_{D_{Ca^{2+}}}$, and the calculated values of the single-channel conductance of the current carried by Ca^{2+} at $[Ca^{2+}]_o = 1.8$ mM (and in the additional presence of 150 mM NaCl and 1.7 mM $MgCl_2$ in the pipette), using Eq. 4, and the fraction of the total current that, under these physiological ion conditions, this Ca^{2+}-carried current represents, using Eq. 5. As an alternative way of judging the goodness of the fit of Eqs. 2–4 to the I-V results in Fig. 11, Fig. 13 plots the single-channel conductance as a function of $a_{Ca_o^{2+}}$, with the slopes of the individual I-V plots superimposed on the computed functions. Fig. 14 shows how the fractional contribution of Ca^{2+} to the total single-channel inward currents grows, from zero to unity, as $a_{Ca_o^{2+}}$ increases, using Eq. 5 and the values shown in Table II.

The "one-ion one-site" notion (on which Eqs. 3 and 4 are based) is not merely an assumption. Rather, such a model fits the data satisfactorily, suggesting that no further sophistication is needed, at least to describe the type of I-V data shown in Fig. 11. Furthermore, in the assayed voltage range, the individual I-V relationships deviate only slightly from straight lines, which justifies our treatment of the single-channel conductances as voltage-independent parameters.

Finally, our approach assumes that the recorded I-V relationships (Fig. 11) extrapolate to the origin regardless of the particular value of the Nernst potential for Ca^{2+}. Indeed, according to Eq. 4, $i_{Ca} = 0$ at $V = 0$ at all $a_{Ca_o^{2+}}$ values, which leads to an expression for the fractional Ca^{2+} current that is independent of voltage (Eq. 5). This expression seems, in principle, at odds with the expected voltage dependence of the fractional Ca^{2+} currents. For example, in the presence of an asymmetrical

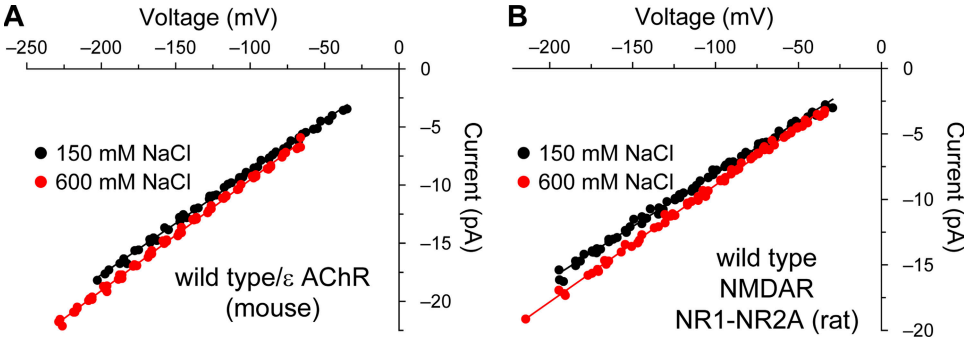

Figure 10. 150 mM Na^+ saturates the permeation pathway of the AChR and the NMDAR. I-V curves recorded in the cell-attached configuration with either 150 or 600 mM NaCl in the pipette solution. For both channels, the pipette solution was pH buffered with 10 mM HEPES/KOH, pH 7.4, and was nominally Ca^{2+} and Mg^{2+} free. (A) Adult mouse wild-type AChR. $\gamma_{150\ mM\ NaCl} = 89 \pm 0.6$ pS; $\gamma_{600\ mM\ NaCl} = 96 \pm 0.5$ pS. (B) NR1-NR2A rat wild-type NMDAR. $\gamma_{150\ mM\ NaCl} = 81 \pm 0.5$ pS; $\gamma_{600\ mM\ NaCl} = 89 \pm 0.5$ pS. To facilitate the visual comparison of slopes, each I-V relationship was displaced along the voltage axis so that it extrapolates to the origin. As expected from nonselective cation channels, the cell-attached curves recorded in the presence of 600 mM NaCl in the pipette were shifted to the right of those recorded with 150 mM NaCl.

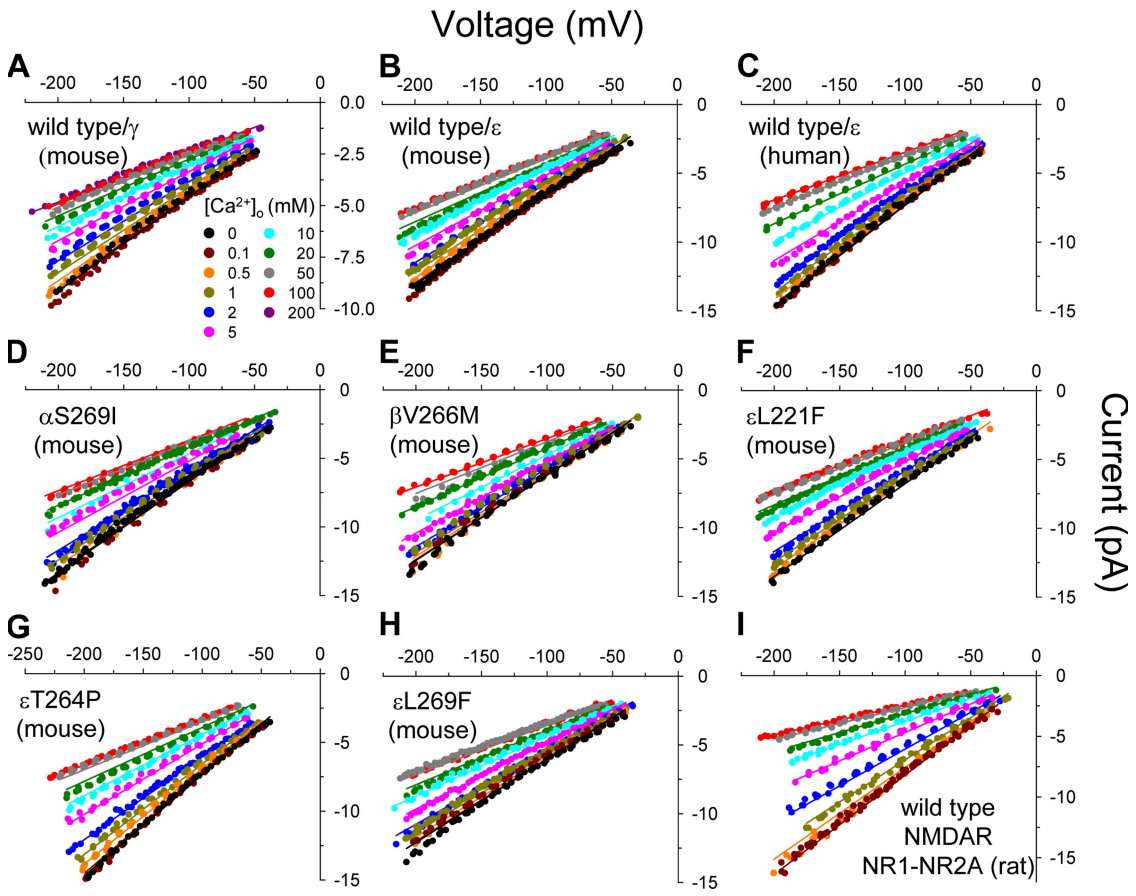

Figure 11. I-V curves recorded in the cell-attached configuration at different values of extracellular $[Ca^{2+}]$. The color code is the same for all panels and is shown in A in terms of Ca^{2+} concentration ($[Ca^{2+}]_o$), rather than Ca^{2+} activity ($a_{Ca_o^{2+}}$). In all cases, the pipette solution also contained 150 mM NaCl (and 10 mM HEPES/KOH, pH 7.4), but only in the case of the wild-type and mutant AChRs did it also contain 1.7 mM $MgCl_2$. The pipette solution used for recordings from the NMDAR was nominally Mg^{2+} free. Recordings from the NMDAR displayed occasional sojourns in an open-channel level of lower conductance, which were excluded from the analysis. Measured current values were fitted as a function of both voltage and $a_{Ca_o^{2+}}$ using Eqs. 2–4, and the values of the estimated parameters are listed in Table II. Hence, the plotted continuous lines are not linear fits to the individual I-V curves. For data fitting, $[Ca^{2+}]_o$ values were expressed as the corresponding Ca^{2+} activities following the work of Butler (1968). Before being fitted, each I-V relationship was displaced along the voltage axis so that it extrapolates to the origin; this was needed to apply Eqs. 2–4. Each panel was fitted independently. The total number of current-voltage-$a_{Ca_o^{2+}}$ data points in each panel was: 496 in A, 657 in B, 507 in C, 490 in D, 420 in E, 557 in F, 444 in G, 532 in H, and 409 in I.

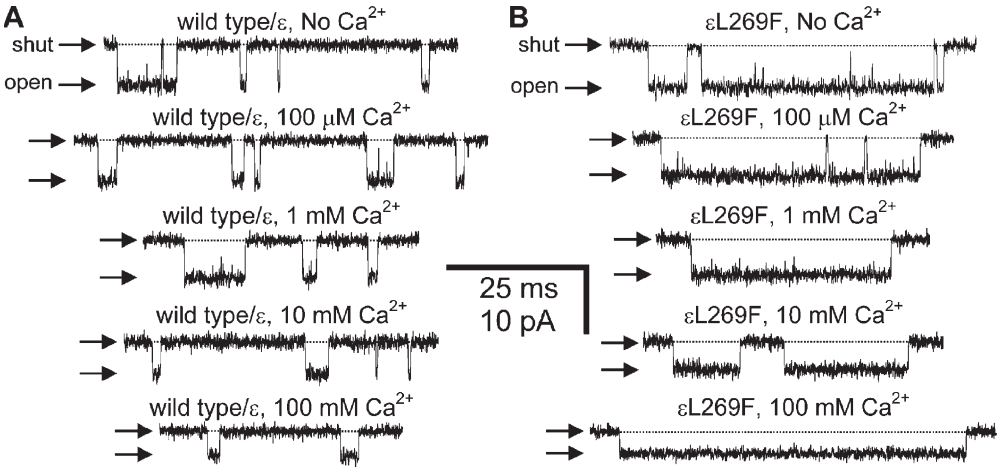

Figure 12. Representative single-channel cell-attached current traces recorded at different values of extracellular $[Ca^{2+}]$. (A) Adult mouse wild-type AChR. (B) Adult mouse AChR harboring the εL269F mutation. In addition to the indicated concentration of Ca^{2+} (as $CaCl_2$), the pipette solution also contained the following (in mM): 150 NaCl, 1.7 $MgCl_2$, and 10 HEPES/KOH, pH 7.4. Applied potential = −100 mV (negative inside the cell). [ACh] ≅ 1 μM. Display f_c ≅ 6 kHz. The zero-current level is indicated on each trace with a dotted line.

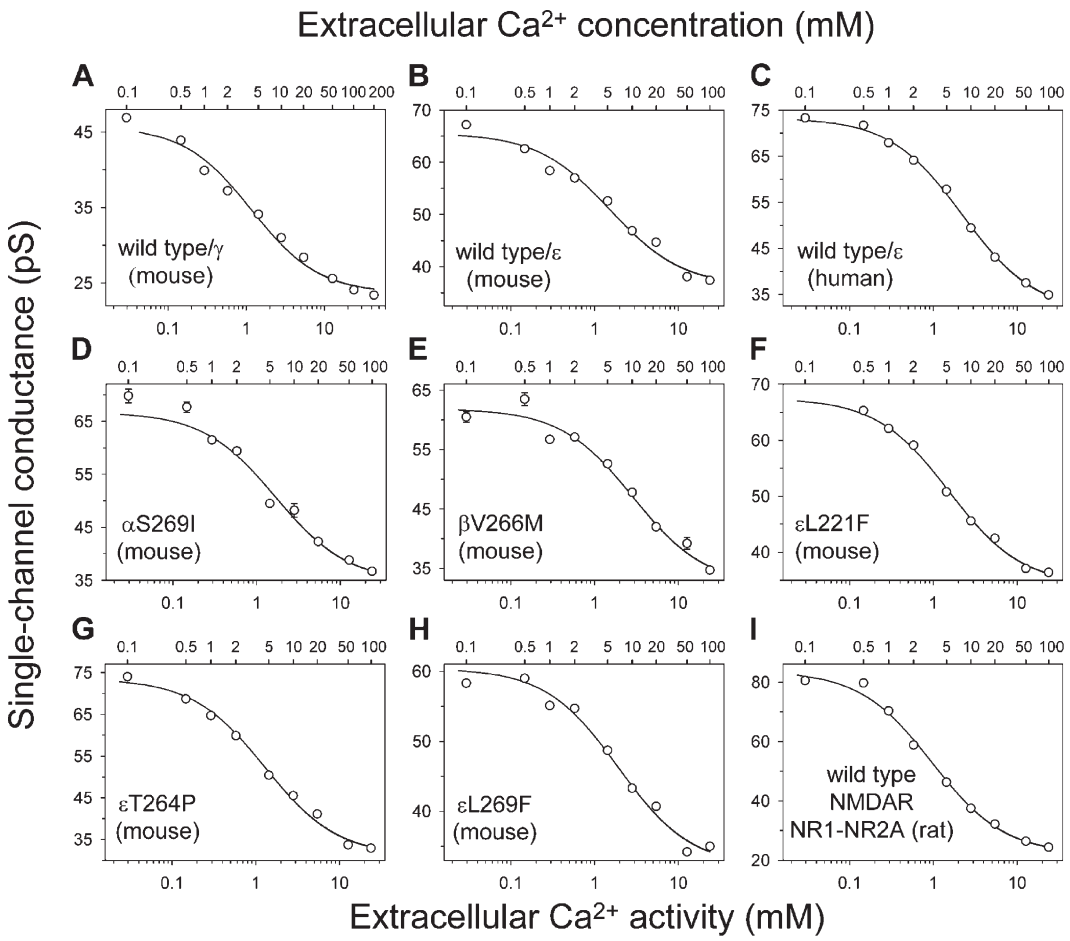

Figure 13. Dependence of single-channel conductance on extracellular Ca^{2+}. The dataset in Fig. 11 is replotted here to better appreciate the quality of the fit of the current-voltage-$a\mathrm{Ca}_o^{2+}$ data with Eqs. 2–4. The symbols correspond to the slopes of the individual I-V curves in Fig. 11, whereas the continuous lines are the computed values of Eq. 2 (divided by voltage) using the estimated parameters in Table II. For most data points, the error bars (standard errors estimated from linear fits to the individual I-Vs) are smaller than the symbols. The points corresponding to zero extracellular Ca^{2+} are, naturally, absent from this type of logarithmic display. Note that the $[Ca^{2+}]_o$ is given in terms of both activity (bottom axes) and concentration (top axes), although only $a\mathrm{Ca}_o^{2+}$ values were used for the fits in Fig. 11.

distribution of Ca^{2+} across the membrane, and a symmetrical distribution of monovalent cations and Mg^{2+}, the fractional Ca^{2+} current must be unity at zero voltage (that is, at the reversal potential of the current carried by the mixture of monovalent cations and Mg^{2+}), and zero at the Nernst potential for Ca^{2+}. Then why are we neglecting this effect of the voltage?

The currents in the I-V plots of Fig. 11 can be regarded as the sum of two components, namely, the current carried by Ca^{2+} and that carried by monovalent cations and Mg^{2+}. Because, in these cell-attached experiments, monovalent cations and Mg^{2+} were distributed rather symmetrically across the membrane, the current carried by these ions reverses at, approximately, zero voltage. Ca^{2+}, on the other hand, was (under most ion conditions) more concentrated on the extracellular side of the membrane, and hence, the Ca^{2+}-carried component of the total current must reverse at positive potentials. As a result, the "net" I-V plots are expected to reverse at a potential that is intermediate between zero and the corresponding Nernst potential for Ca^{2+}. Although these cell-attached I-V curves did not display any marked deviation from linearity in the voltage range tested, this off-zero reversal potential may manifest as a displacement of the I-V straight line along the voltage axis in the depolarizing direction. Evidently, the larger this displacement is, the more invalid the expressions in Eqs. 4 and 5 are. To quantify this phenomenon in the most unequivocal manner possible, we recorded single-channel I-V curves in the outside-out configuration in the presence of (saturating) 100 mM Ca^{2+} on the extracellular side and a nominally Ca^{2+}-free solution on the cytoplasmic side of the channel (both solutions also contained 150 mM NaCl and 1.7 mM $MgCl_2$; Fig. 15). This asymmetrical distribution of Ca^{2+} across the membrane mimics the most asymmetrical ion condition assayed in the cell-attached experiments illustrated in Fig. 11 (with the exception of the cell-attached recordings from

TABLE II

Interaction between Ca^{2+} and the Channel's Pore in the AChR and NMDAR

Construct	$\gamma_{Na^+\text{-}Mg^{2+}}$ (pS)[a]	$\gamma_{Ca^{2+}}$ (pS)[b]	$K_{D_{Ca^{2+}}}$ (mM; activity)[c]	$K_{D'_{Ca^{2+}}}$ (mM; concentration)[d]	Physiological Ca^{2+} conductance (pS)[e]	Physiological fractional Ca^{2+} current (%)[f]
wild-type/γ AChR (fetal, mouse)	46 ± 0.1	24 ± 0.1	1.16 ± 0.04	4.0	7.5 ± 0.2	19.3 ± 0.5
wild-type/ε AChR (adult, mouse)	66 ± 0.1	36 ± 0.2	1.53 ± 0.05	5.3	9.4 ± 0.2	16.3 ± 0.5
wild-type/ε AChR (adult, human)	73 ± 0.1	31 ± 0.2	2.22 ± 0.05	7.9	6.1 ± 0.1	9.3 ± 0.2
αS269I (adult, mouse)	67 ± 0.2	35 ± 0.3	1.68 ± 0.06	5.9	8.4 ± 0.2	14.3 ± 0.4
βV266M (adult, mouse)	62 ± 0.2	32 ± 0.4	2.88 ± 0.13	10	5.0 ± 0.2	8.8 ± 0.4
εL221F (adult, mouse)	68 ± 0.1	34 ± 0.2	1.54 ± 0.03	5.4	8.8 ± 0.1	15.0 ± 0.3
εT264P (adult, mouse)	74 ± 0.2	31 ± 0.2	1.29 ± 0.03	4.5	9.1 ± 0.1	15.0 ± 0.3
εL269F (adult, mouse)	61 ± 0.2	32 ± 0.2	1.92 ± 0.07	6.8	7.0 ± 0.2	13.0 ± 0.4
wild-type NR1-NR2A (rat)	84 ± 0.2	22 ± 0.3	0.96 ± 0.02	3.3	7.9 ± 0.1	12.8 ± 0.3

[a]Single-channel conductance in a nominally Ca^{2+}-free extracellular solution containing the following (in mM): 150 NaCl, 1.7 $MgCl_2$, and 10 HEPES/KOH, pH 7.4. $MgCl_2$ was omitted in the case of the recordings from rat NR1-NR2A NMDARs (see Results). This parameter, as well as $\gamma_{Ca^{2+}}$ and $K_{D_{Ca^{2+}}}$, were estimated from the fit of the data in Fig. 11 with Eqs. 2–4.

[b]Single-channel conductance in the presence of saturating extracellular Ca^{2+}.

[c]Apparent dissociation equilibrium constant of Ca^{2+} from the (phenomenologically defined) cation-binding site in the channel's pore in the presence of 150 mM extracellular Na^+ and, in the case of the wild-type and mutant AChRs, 1.7 mM extracellular Mg^{2+}. The values are expressed in terms of activity.

[d]Apparent dissociation equilibrium constant of Ca^{2+} expressed in terms of concentration.

[e]Single-channel conductance of the Ca^{2+}-carried component of the total currents in the presence of $[Ca^{2+}]_o$ = 1.8 mM, calculated by dividing Eq. 4 by voltage. Errors were calculated by propagating the errors of the appropriate variables in Eq. 4, assuming that these are independent of each other, and that they are normally distributed.

[f]Fractional contribution of the Ca^{2+} current to the total current in the presence of $[Ca^{2+}]_o$ = 1.8 mM, calculated using Eq. 5. Errors were calculated by propagating the errors of the appropriate variables in this equation, assuming that these are independent of each other, and that they are normally distributed.

the fetal-type AChR, in which case the highest $[Ca^{2+}]_o$ was 200 mM). It should be noted here that the voltage-axis intercepts of cell-attached I-V plots are not very informative because of the uncertainty as to the exact value of the cell's membrane potential, which is not necessarily zero even if, as was the case for these experiments, the cells are bathed in an isotonic KCl-based solution. Fig. 15 shows that, in the outside-out configuration and with a 100-mM outside/nominally free inside Ca^{2+} gradient, the projection of the (linear) I-V curve crosses the voltage axis at ∼+18 mV. That is, at any hyperpolarized potential, the current (carried exclusively by Ca^{2+}, at this saturating Ca^{2+} concentration) is larger than it would be if the I-V curve crossed the voltage axis at the origin. Because 100 mM is higher than the $[Ca^{2+}]_o$ values used for most other I-V curves shown in Fig. 11, this 18-mV rightward displacement of the I-V relationship represents an upper bound. In other words, the voltage shift corresponding to the Ca^{2+} component of the total current is expected to be much smaller at most other values of $[Ca^{2+}]_o$ tested, and certainly at the physiological value of 1.8 mM. It can be seen, then, that the lower the $[Ca^{2+}]_o$ and the more hyperpolarized the membrane potential, the more valid Eq. 4 (and thus, the more negligible the voltage dependence of the fractional Ca^{2+} current). We conclude that, if anything, by assuming the validity of Eq. 4 at all voltages and $[Ca^{2+}]_o$ values, our approach may somewhat underestimate the contribution of physiological Ca^{2+} to the total cation current at physiological membrane potentials.

Our estimate of the fractional Ca^{2+} current through the muscle AChR (be it human or mouse, fetal or adult type, wild type or mutant) is in the ∼10–20% range (Table II), which is higher than values previously reported in the literature using the simultaneous measurement of whole cell currents and Ca^{2+} influx, under comparable ion and voltage conditions (Vernino et al., 1994; Ragozzino et al., 1998; Fucile et al., 2006). To investigate whether our single-channel method systematically overestimates the contribution of Ca^{2+} to the total currents, we estimated the fractional Ca^{2+} current through the rat NMDAR composed of NR1 and NR2A subunits also transiently expressed in HEK-293 cells, but in the nominal absence of external Mg^{2+} to avoid

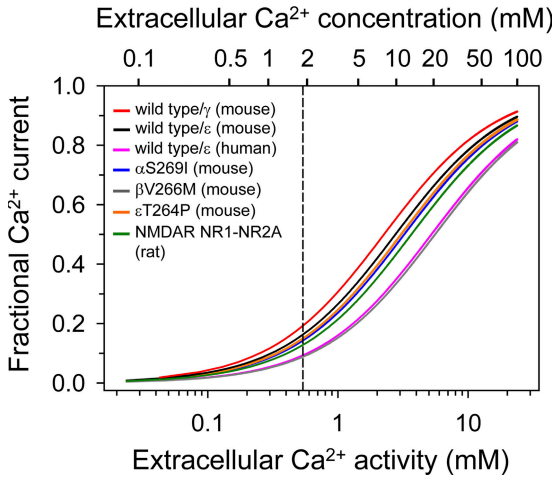

Figure 14. Dependence of fractional Ca^{2+} currents on extracellular Ca^{2+}. Eq. 5 was computed for the different constructs using the estimated parameters in Table II. The vertical dashed line indicates the physiological value of $[Ca^{2+}]_o$ = 1.8 mM. For clarity, the data corresponding to two of the AChR mutants (εL221 and εL269F) are omitted from this plot.

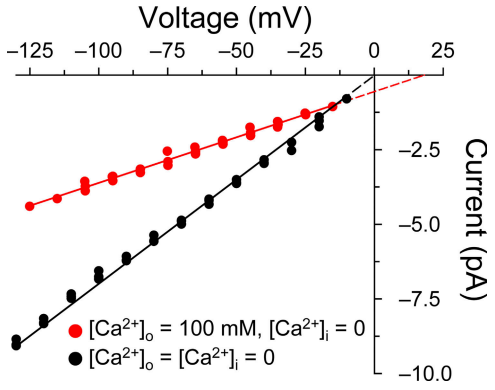

Figure 15. I-V curves recorded in the outside-out configuration in the presence and absence of Ca^{2+} on the extracellular side. I-V curves from the εT264P mutant were recorded with (in mM) 150 NaCl, 1.7 $MgCl_2$, and 10 HEPES/KOH, pH 7.4, bathing both sides of the channel. Red symbols correspond to the curve recorded in the additional presence of 100 mM (concentration) Ca^{2+} on the extracellular side (data from three patches). At this saturating concentration of Ca^{2+}, the inward currents are almost exclusively carried by Ca^{2+}. Black symbols correspond to the curve recorded in the absence of added Ca^{2+} (data from three patches). The projections of the straight lines fitted to the plots (dashed lines) intercept the voltage axis at zero (no Ca^{2+} added) and +18 mV ($[Ca^{2+}]_o$ = 100 mM), as expected from a nonselective cation channel with measurable permeability to Ca^{2+}. The value of the reversal potential at $[Ca^{2+}]_o$ = 100 mM, however, may well be more depolarized than the indicated intercept. The slopes are (69.8 ± 0.8) pS at $[Ca^{2+}]_o$ = 0 and (30.6 ± 0.6) pS at $[Ca^{2+}]_o$ = 100 mM. The displacement along the voltage axis of the Ca^{2+}-carried component of the total current at the physiological value of $[Ca^{2+}]_o$ = 1.8 mM (and in the presence of Na^+ and Mg^{2+}) is expected to be much smaller than that at $[Ca^{2+}]_o$ = 100 mM. In these outside-out experiments, the reference Ag/AgCl wire was connected to the bath solution through an agar bridge containing 200 mM KCl. Liquid-junction potentials were corrected as described previously (Barry and Lynch, 1991; Barry, 1994).

channel block (Ascher and Nowak, 1988). We chose this receptor as a control because the fraction of the current carried by Ca^{2+} has been investigated in detail for this channel, perhaps more thoroughly than for any other nonselective cation channel. Analysis of the data in Fig. 11 I yielded the corresponding ion-conduction parameters (Table II), which lead to the estimates of ∼7.9 pS for the Ca^{2+}-carried conductance at $[Ca^{2+}]_o$ = 1.8 mM and of ∼13% for the corresponding fractional Ca^{2+} current. The value of the fractional Ca^{2+} current is in excellent agreement with those measured by Neher, Sakmann, and coworkers (11%; Burnashev et al., 1995), Wollmuth and coworkers (13.5%; Jatzke et al., 2002), and Egan and Khakh (14%; Egan and Khakh, 2004) applying the fluorimetry/patch clamp approach under virtually identical ion and voltage conditions to the same NMDAR subunit combination expressed in the same cell line. Thus, although the reasons for the discrepant estimates of the fractional Ca^{2+} currents in the case of the muscle AChR remain a puzzle, the close agreement in the case of the NMDAR is highly reassuring. As mentioned above, the difficulties associated with the combined whole cell current/Ca^{2+}-influx measurements have long been recognized (Zhou and Neher, 1993; Rogers and Dani, 1995; Schneggenburger, 1996).

DISCUSSION

AChR Desensitization during Deactivation: Impact on In Vivo Function and on Structure–Function Relationships

Here, we showed that the response of a panel of slow-channel syndrome AChR mutants to pulses of ACh of nearly physiological duration and delivered at physiological frequencies diminishes along the trains in a manner that is consistent with the AChR entering desensitized conformations upon ACh removal. It is difficult, however, to predict the extent to which this decremental response contributes to the patients' impaired neuromuscular transmission without further experiments. This difficulty arises from the fact that, in an outside-out experiment, the entire population of receptor channels in the patch is exposed to each pulse of ACh, whereas, in the intact neuromuscular junction, only a subset of the postsynaptic receptors is thought to interact with the quanta released upon the arrival of each action potential (Hartzell et al., 1975; Salpeter, 1987; Barbour and Häusser, 1997). Because it is unlikely that exactly the same subset of AChRs is activated every time ACh is released from the motor neuron (that is, the subsets of successively activated receptors are unlikely to overlap fully), the frequency at which each individual AChR is exposed to ACh during synaptic transmission must, inevitably, be lower than that of the

train of incoming action potentials. And because the extent of depression is frequency dependent (Fig. 6), lower frequencies mean less depression. However, the exact extent to which subsets of AChRs activated by successive ACh pulses overlap in vivo, and thus the "effective" frequency at which each AChR is activated, remains unknown; hence the need for further experiments under conditions that recreate synaptic transmission more closely than a fast-perfused outside-out patch of membrane. It is worth mentioning here that synaptic depression due to receptor desensitization during deactivation (that is, upon neurotransmitter removal) has been proposed to play a physiological role in several central glutamatergic synapses (Trussell et al., 1993; Otis et al., 1996; Turecêk and Trussell, 2000; Chen et al., 2002). Therefore, in the absence of further information, we would not rule out the occurrence of this phenomenon during neuromuscular transmission in slow-channel syndrome patients.

What can be said without a doubt, however, is that the observed decremental response of slow-channel AChRs to repetitive stimulation is not predicted by the type of kinetic schemes that have been used, thus far, to understand what is wrong with these receptors. These kinetic models ignore desensitization as a pathway for burst termination, and thus, are likely to be misleading. For example, let us consider a hypothetical mutation that increases the gating equilibrium constant by a factor of $\sim$50 (that is, $\Delta\Delta G^{o} \cong 2.3$ kcal mol^{-1}, not an uncommon finding) and does not affect the kinetics of ACh association to and dissociation from the transmitter-binding sites or the kinetics of entry into and recovery from desensitization. Let us further suppose that the mutation occurs at a position of the protein such that the 50-fold increase in the $CA_2 \rightleftharpoons OA_2$ equilibrium constant results in an opening rate constant that is faster than the wild type's by a factor of $\sim$3, and a closing rate constant that is slower by a factor of $\sim$17 (as would be the case for a mutation at a site of the protein with a Φ-value of $\sim$0.3; Grosman et al., 2000; Grosman, 2003). Hence, taking mouse muscle, adult wild-type values (Salamone et al., 1999; Grosman and Auerbach, 2001; Elenes et al., 2006) of 50,000 s^{-1} for the diliganded AChR opening rate constant (that is, β_2 in Fig. 1), 2,000 s^{-1} for the diliganded AChR closing rate constant (α_2), 50,000 s^{-1} for the ACh-dissociation rate constant from the diliganded closed receptor ($2k_-$), 10 s^{-1} for the ACh-dissociation rate constant from the diliganded open receptor ($2j_-$), and 25 s^{-1} for the rate of entry into desensitization (D_+), the mean duration of a burst of ACh-diliganded openings for this hypothetical mutant would be $\sim$15.5 ms (calculated using Eq. 1) instead of the $\sim$34-ms duration (calculated using the expression $(1+\beta_2/2k_-)/\alpha_2$) that would be expected from such a channel if entry into desensitization (and, to a much lesser extent, ACh dissociation from the open state) did not contribute to the termination of bursts. It is difficult, then, to envision how the estimates of rate constants obtained from kinetic analysis of electrophysiological data (and, perhaps more importantly, the mechanistic insight derived from them) could be correct when desensitization is not explicitly included in the kinetic models, especially as the gain-of-function phenotype becomes more pronounced. The reason why desensitized states have generally been omitted is not entirely clear to us, but we surmise that this might have to do with the fact that the effect of desensitization on burst termination is much less obvious during the steady application of agonist that occurs in (the much more common) cell-attached experiments than upon the application of trains of agonist pulses (our Fig. 4, for example). This highlights the extreme importance of analyzing kinetic data obtained under both equilibrium and nonequilibrium conditions. Evidently, meaningful structure–function relationships hinge on the use of adequate kinetic models.

Finally, we would like to emphasize that earlier work with the muscle AChR has firmly established that patch excision does not affect the kinetics of this channel, at least not to a degree that would invalidate the conclusions from our outside-out experiments. For example, a comparison of the mean duration of bursts of diliganded openings estimated from cell-attached single-channel recordings and of the deactivation time constants estimated from outside-out concentration-jump experiments (like those illustrated here in Figs. 3 A and 8 A), for the wild-type and several mutant AChRs, revealed a close correspondence between these two sets of values (see Fig. 2 B in Elenes et al., 2006). If anything, the mean durations estimated from cell-attached experiments turned out to be a little longer for some of the constructs, suggesting that the contribution of desensitization to the time course of deactivation could be even more pronounced if the integrity of the cytoplasm were preserved.

Ca^{2+} Currents through the Muscle AChR: New Method, New Results

In this paper, we addressed the issue of the Ca^{2+} permeability through the AChR using a simple, yet novel electrophysiological approach. Our method relies on single-channel recordings, requires far fewer controls and calibrations than the combined use of whole cell current and intracellular Ca^{2+} measurements (Thayer et al., 1988; Neher and Augustine, 1992; Zhou and Neher, 1993; Vernino et al., 1994; Schneggenburger, 1996), and does not resort to the calculation of permeability ratios from reversal-potential estimates (using the Goldman-Hodgkin-Katz voltage equation). Indeed, making physical sense out of $P_{Ca^{2+}}/P_X$ permeability ratios in terms of fractional Ca^{2+} currents or the single-channel conductance of the Ca^{2+}-carried component of the total currents, under physiological ion and voltage conditions, is seldom straightforward.

A comparison of the values in the two rightmost columns of Table II among the different wild-type and mutant AChRs tested indicates that the differences are small. This is particularly clear if we focus our comparison on the values of the "physiological Ca^{2+} conductance" (rather than on the less physiologically relevant fractional Ca^{2+} currents) and consider the additional layer of complexity that variable levels of protein expression contribute to the problem of the amount of Ca^{2+} entering the postsynaptic cell upon channel activation. This result suggests that the increased influx of Ca^{2+} through the slow-channel mutants examined here would be due, mainly, to the slower decay of the endplate currents that they mediate, rather than to an increased ability of these channels to conduct Ca^{2+}.

Also, quite unexpectedly, we found that the muscle AChR conducts nearly as much Ca^{2+} as the NR1-NR2A NMDAR, with Ca^{2+}-specific conductance values of 7.5, 9.4, and 6.1 pS for the fetal mouse, adult mouse, and adult human AChRs, respectively, and 7.9 pS for the NMDAR (Table II). This is remarkable because previous studies on the muscle-type AChR have reported much lower values (for example, Decker and Dani, 1990; Vernino et al., 1994), which contributed to the idea that the NMDAR is the largest source of neurotransmitter-gated Ca^{2+} entry into the cell. It is, thus, intriguing to ponder that cation permeation through the muscle AChR might play a physiological role in phenomena other than motor-endplate depolarization, just as is the case for the NMDAR in central synapses. It would be interesting to apply our method to the AChR subtypes that are expressed in nonmuscle tissues, where the effect of AChR-mediated cytosolic Ca^{2+} elevation on neurotransmitter release (in presynaptic neurons; for example, McKay et al., 2007) and on the pathogenesis of cancer (in several epithelia; for example, Cattaneo et al., 1997) has been documented.

The similarities between the muscle AChR and the NMDAR (as far as their divalent cation permeation properties are concerned) do not extend much beyond their nearly identical Ca^{2+}-conduction rates, though. Whereas the NMDAR discriminates strongly between Ca^{2+} and Mg^{2+}, in a way that defines this receptor channel's physiological role, it makes hardly a difference to the muscle AChR whether it is Ca^{2+} or Mg^{2+} that is going through.

We thank J. Gasser, G. Papke, and C. Staehlin for technical assistance, and L.G. Sivilotti (University College London), S.M. Sine (Mayo Clinic College of Medicine), and J. Woodward (Medical University of South Carolina) for cDNA clones.

This work was supported by National Institutes of Health grant RO1 NS042169 to C. Grosman.

Edward N. Pugh Jr. served as editor.

Submitted: 24 July 2008
Accepted: 5 January 2009

REFERENCES

Ascher, P., and L. Nowak. 1988. The role of divalent cations in the *N*-methyl-D-aspartate responses of mouse central neurones in culture. *J. Physiol.* 399:247–266.

Auerbach, A., and G. Akk. 1998. Desensitization of mouse nicotinic acetylcholine receptor channels. A two-gate mechanism. *J. Gen. Physiol.* 112:181–197.

Barbour, B., and M. Häusser. 1997. Intersynaptic diffusion of neurotransmitter. *Trends Neurosci.* 20:377–384.

Barry, P.H. 1994. JPCalc, a software package for calculating liquid junction potential corrections in patch-clamp, intracellular, epithelial and bilayer measurements and for correcting junction potential measurements. *J. Neurosci. Methods.* 51:107–116.

Barry, P.H., and J.W. Lynch. 1991. Liquid junction potentials and small cell effects in patch-clamp analysis. *J. Membr. Biol.* 121:101–117.

Bertrand, D., J.L. Galzi, A. Devillers-Thiéry, S. Bertrand, and J.P. Changeux. 1993. Mutations at two distinct sites within the channel domain M2 alter calcium permeability of neuronal α7 nicotinic receptor. *Proc. Natl. Acad. Sci. USA.* 90:6971–6975.

Brownlow, S., R. Webster, R. Croxen, M. Brydson, B. Neville, J.-P. Lin, A. Vincent, J. Newsom-Davis, and D. Beeson. 2001. Acetylcholine receptor δ subunit mutations underlie a fast-channel myasthenic syndrome and arthrogryposis multiplex congenita. *J. Clin. Invest.* 108:125–130.

Burnashev, N., Z. Zhou, E. Neher, and B. Sakmann. 1995. Fractional calcium currents through recombinant GluR channels of the NMDA, AMPA and kainate receptor subtypes. *J. Physiol.* 485:403–418.

Butler, J.M. 1968. The thermodynamic activity of calcium in sodium chloride-calcium chloride electrolytes. *Biophys. J.* 8:1426–1433.

Cattaneo, M.G., F. D'Atri, and L.M. Vicentini. 1997. Mechanisms of mitogen-activated protein kinase activation by nicotine in small-cell lung carcinoma cells. *Biochem. J.* 328:499–503.

Chen, C., D.M. Blitz, and W.G. Regehr. 2002. Contributions of receptor desensitization and saturation to plasticity at the retinogeniculate synapse. *Neuron.* 33:779–788.

Colquhoun, D., and A.G. Hawkes. 1982. On the stochastic properties of bursts of single ion channel openings and of clusters of bursts. *Philos. Trans. R. Soc. Lond. B Biol. Sci.* 300:1–89.

Colquhoun, D., and B. Sakmann. 1985. Fast events in single-channel currents activated by acetylcholine and its analogues at the frog muscle end-plate. *J. Physiol.* 369:501–557.

Colquhoun, D., A.G. Hawkes, A. Merlushkin, and B. Edmonds. 1997. Properties of single ion channel currents elicited by a pulse of agonist concentration or voltage. *Philos. Trans. R. Soc. Lond. A.* 355:1743–1786.

Corringer, P.-J., S. Bertrand, J.-L. Galzi, A. Devillers-Thiéry, J.-P. Changeux, and D. Bertrand. 1999. Mutational analysis of the charge selectivity filter of the α7 nicotinic acetylcholine receptor. *Neuron.* 22:831–843.

Croxen, R., C. Newland, D. Beeson, H. Oosterhuis, G. Chauplannaz, A. Vincent, and J. Newsom-Davis. 1997. Mutations in different functional domains of the human muscle acetylcholine receptor alpha subunit in patients with the slow-channel congenital myasthenic syndrome. *Hum. Mol. Genet.* 6:767–774.

Croxen, R., C. Hatton, C. Shelley, M. Brydson, G. Chauplannaz, H. Oosterhuis, A. Vincent, J. Newsom-Davis, D. Colquhoun, and D. Beeson. 2002. Recessive inheritance and variable penetrance of slow-channel congenital myasthenic syndromes. *Neurology.* 59:162–168.

Decker, E.R., and J.A. Dani. 1990. Calcium permeability of the nicotinic acetylcholine receptor: the single-channel calcium influx is significant. *J. Neurosci.* 10:3413–3420.

Di Castro, A., K. Martinello, F. Grassi, F. Eusebi, and A.G. Engel. 2007. Pathogenic point mutations in a transmembrane domain of the ε subunit increase the Ca^{2+} permeability of the human endplate ACh receptor. *J. Physiol.* 579:671–677.

Edmonds, B., A.J. Gibb, and D. Colquhoun. 1995. Mechanisms of activation of muscle nicotinic acetylcholine receptors and the time course of endplate currents. *Annu. Rev. Physiol.* 57:469–493.

Egan, T.M., and B.S. Khakh. 2004. Contribution of calcium ions to P2X channel responses. *J. Neurosci.* 24:3413–3420.

Elenes, S., Y. Ni, G.D. Cymes, and C. Grosman. 2006. Desensitization contributes to the synaptic response of gain-of-function mutants of the muscle nicotinic receptor. *J. Gen. Physiol.* 128:615–627.

Engel, A.G., K. Ohno, M. Milone, H.-L. Wang, S. Nakano, C. Bouzat, J.N. Pruitt II, D.O. Hutchinson, J.M. Brengman, N. Bren, et al. 1996. New mutations in acetylcholine receptor subunit genes reveal heterogeneity in the slow-channel congenital myasthenic syndrome. *Hum. Mol. Genet.* 5:1217–1227.

Engel, A.G., K. Ohno, and S.M. Sine. 2003. Sleuthing molecular targets for neurological diseases at the neuromuscular junction. *Nat. Rev. Neurosci.* 4:339–352.

Fucile, S., A. Sucapane, F. Grassi, F. Eusebi, and A.G. Engel. 2006. The human adult subtype ACh receptor channel has high Ca^{2+} permeability and predisposes to endplate Ca^{2+} overloading. *J. Physiol.* 573:35–43.

Galzi, J.-L., A. Devillers-Thiéry, N. Hussy, S. Bertrand, J.-P. Changeux, and D. Bertrand. 1992. Mutations in the channel domain of a neuronal nicotinic receptor convert ion selectivity from cationic to anionic. *Nature.* 359:500–505.

Gomez, C.M., and J.T. Gammack. 1995. A leucine-to-phenylalanine substitution in the acetylcholine receptor ion channel in a family with the slow-channel syndrome. *Neurology.* 45:982–985.

Gomez, C.M., R. Maselli, J.E. Gundeck, M. Chao, J.W. Day, S. Tamamizu, J.A. Lasalde, M. McNamee, and R.L. Wollmann. 1997. Slow-channel transgenic mice: a model of postsynaptic organellar degeneration at the neuromuscular junction. *J. Neurosci.* 17:4170–4179.

Groshong, J.S., M.J. Spencer, B.J. Bhattacharyya, E. Kudrryashova, B.P.S. Vohra, R. Zayas, R.L. Wollmann, R.J. Miller, and C.M. Gomez. 2007. Calpain activation impairs neuromuscular transmission in a mouse model of the slow-channel myasthenic syndrome. *J. Clin. Invest.* 117:2903–2912.

Grosman, C. 2003. Free-energy landscapes of ion-channel gating are malleable: changes in the number of bound ligands are accompanied by changes in the location of the transition state in acetylcholine-receptor channels. *Biochemistry.* 42:14977–14987.

Grosman, C., and A. Auerbach. 2000. Asymmetric and independent contribution of the second transmembrane segment 12′ residues to diliganded gating of acetylcholine receptor channels. A single-channel study with choline as the agonist. *J. Gen. Physiol.* 115:637–651.

Grosman, C., and A. Auerbach. 2001. The dissociation of acetylcholine from open nicotinic receptor channels. *Proc. Natl. Acad. Sci. USA.* 98:14102–14107.

Grosman, C., M. Zhou, and A. Auerbach. 2000. Mapping the conformational wave of acetylcholine receptor channel gating. *Nature.* 403:773–776.

Hantai, D., P. Richard, J. Koenig, and B. Eymard. 2004. Congenital myasthenic syndromes. *Curr. Opin. Neurol.* 17:539–551.

Hartzell, H.C., S.W. Kuffler, and D. Yoshikami. 1975. Post-synaptic potentiation: interaction between quanta of acetylcholine at the skeletal neuromuscular synapse. *J. Physiol.* 251:427–463.

Hatton, C., C. Shelley, M. Brydson, D. Beeson, and D. Colquhoun. 2003. Properties of the human muscle nicotinic receptor, and of the slow-channel syndrome mutant εL221F, inferred from maximum likelihood fits. *J. Physiol.* 547:729–760.

Hennig, R., and T. Lømo. 1985. Firing patterns of motor units in normal rats. *Nature.* 314:164–166.

Hollmann, M., J. Boulter, C. Maron, L. Beasley, J. Sullivan, G. Pecht, and S. Heinemann. 1993. Zinc potentiates agonist-induced currents at certain splice variants of the NMDA receptor. *Neuron.* 10:943–954.

Jatzke, C., J. Watanabe, and L.P. Wollmuth. 2002. Voltage and concentration dependence of Ca^{2+} permeability in recombinant glutamate receptor subtypes. *J. Physiol.* 538:25–39.

Jonas, P. 1995. Fast application of agonists to isolated membrane patches. *In* Single-Channel Recording. B. Sakmann and E. Neher, editors. Plenum Press, New York. 213–243.

Leonard, J.P., and M.M. Salpeter. 1979. Agonist-induced myopathy at the neuromuscular junction is mediated by calcium. *J. Cell Biol.* 82:811–819.

McKay, B.E., A.N. Placzek, and J.A. Dani. 2007. Regulation of synaptic transmission and plasticity by neuronal nicotinic acetylcholine receptors. *Biochem. Pharmacol.* 74:1120–1133.

Neher, E., and G.J. Augustine. 1992. Calcium gradients and buffers in bovine chromaffin cells. *J. Physiol.* 450:273–301.

Ohno, K., D.O. Hutchinson, M. Milone, J.M. Brengman, C. Bouzat, S.M. Sine, and A.G. Engel. 1995. Congenital myasthenic syndrome caused by prolonged acetylcholine receptor channel openings due to a mutation in the M2 domain of the epsilon subunit. *Proc. Natl. Acad. Sci. USA.* 92:758–762.

Ohno, K., H.-L. Wang, M. Milone, N. Bren, J.M. Brengman, S. Nakano, P. Quiram, J.N. Pruitt, S.M. Sine, and A.G. Engel. 1996. Congenital myasthenic syndrome caused by decreased agonist binding due to a mutation in the acetylcholine receptor ε subunit. *Neuron.* 17:157–170.

Otis, T., S. Zhang, and L.O. Trussell. 1996. Direct measurement of AMPA receptor desensitization induced by glutamatergic synaptic transmission. *J. Neurosci.* 16:7496–7504.

Purohit, Y., and C. Grosman. 2006. Estimating binding affinities of the nicotinic receptor for low-efficacy ligands using mixtures of agonists and two-dimensional concentration–response relationships. *J. Gen. Physiol.* 127:719–735.

Qin, F. 2004. Restoration of single-channel currents using the segmental *k*-means method based on Hidden Markov modeling. *Biophys. J.* 86:1488–1501.

Qin, F., A. Auerbach, and F. Sachs. 1996. Estimating single-channel kinetic parameters from idealized patch-clamp data containing missed events. *Biophys. J.* 70:264–280.

Ragozzino, D., B. Barabino, S. Fucile, and F. Eusebi. 1998. Ca^{2+} permeability of mouse and chick nicotinic acetylcholine receptors expressed in transiently transfected human cells. *J. Physiol.* 507:749–757.

Reitstetter, R., R.J. Lukas, and R. Gruener. 1999. Dependence of nicotinic acetylcholine receptor recovery from desensitization on the duration of agonist exposure. *J. Pharmacol. Exp. Ther.* 289:656–660.

Robinson, R.A., and R.H. Stokes. 1955. Electrolyte Solutions. Butterworths Scientific Publications, London. 512 pp.

Rogers, M., and J.A. Dani. 1995. Comparison of quantitative calcium flux through NMDA, ATP, and ACh receptor channels. *Biophys. J.* 68:501–506.

Salamone, F.N., M. Zhou, and A. Auerbach. 1999. A re-examination of adult mouse nicotinic acetylcholine receptor channel activation kinetics. *J. Physiol.* 516:315–330.

Salpeter, M.M. 1987. Vertebrate neuromuscular junctions: general morphology, molecular organization, and functional consequences. *In* The Vertebrate Neuromuscular Junction. M.M. Salpeter, editor. Alan R. Liss, Inc., New York. 1–54.

Schneggenburger, R. 1996. Simultaneous measurement of Ca^{2+} influx and reversal potentials in recombinant *N*-methyl-D-aspartate receptor channels. *Biophys. J.* 70:2165–2174.

Schneggenburger, R., Z. Zhou, A. Konnerth, and E. Neher. 1993. Fractional contribution of calcium to the cation current through glutamate receptor channels. *Neuron*. 11:133–143.

Thayer, S.A., M. Sturek, and R.J. Miller. 1988. Measurement of neuronal Ca^{2+} transients using simultaneous microfluorimetry and electrophysiology. *Pflugers Arch*. 412:216–223.

Trussell, L.O., S. Zhang, and I.M. Raman. 1993. Desensitization of AMPA receptors upon multiquantal neurotransmitter release. *Neuron*. 10:1185–1196.

Tureĉek, R., and L.O. Trussell. 2000. Control of synaptic depression by glutamate transporters. *J. Neurosci.* 20:2054–2063.

Vernino, S., M. Rogers, K.A. Radcliffe, and J.A. Dani. 1994. Quantitative measurement of calcium flux through muscle and neuronal nicotinic acetylcholine receptors. *J. Neurosci.* 14:5514–5524.

Wyllie, D.J.A., P. Béhé, and D. Colquhoun. 1998. Single-channel activations and concentration jumps: comparison of recombinant NR1a/NR2A and NR1a/NR2D NMDA receptors. *J. Physiol.* 510:1–18.

Zhou, Z., and E. Neher. 1993. Calcium permeability of nicotinic acetylcholine receptor channels in bovine adrenal chromaffin cells. *Pflugers Arch*. 425:511–517.